

University of New Hampshire

## University of New Hampshire Scholars' Repository

---

Master's Theses and Capstones

Student Scholarship

---

Winter 2011

### Reconstructing the variability in the Indian Monsoon from the last glacial period to present

Sarah Arianne Schulenberg

*University of New Hampshire, Durham*

Follow this and additional works at: <https://scholars.unh.edu/thesis>

---

#### Recommended Citation

Schulenberg, Sarah Arianne, "Reconstructing the variability in the Indian Monsoon from the last glacial period to present" (2011). *Master's Theses and Capstones*. 694.

<https://scholars.unh.edu/thesis/694>

This Thesis is brought to you for free and open access by the Student Scholarship at University of New Hampshire Scholars' Repository. It has been accepted for inclusion in Master's Theses and Capstones by an authorized administrator of University of New Hampshire Scholars' Repository. For more information, please contact [Scholarly.Communication@unh.edu](mailto:Scholarly.Communication@unh.edu).

RECONSTRUCTING THE VARIABILITY IN THE INDIAN MONSOON  
FROM THE LAST GLACIAL PERIOD TO PRESENT

BY

SARAH ARIANNE SCHULENBERG  
Bachelor of Science, Missouri State University, 2007

THESIS

Submitted to the University of New Hampshire  
in Partial Fulfillment of  
the Requirements for the Degree of

Master of Science  
in  
Earth Sciences: Oceanography

December 2011

UMI Number: 1507833

All rights reserved

INFORMATION TO ALL USERS

The quality of this reproduction is dependent upon the quality of the copy submitted.

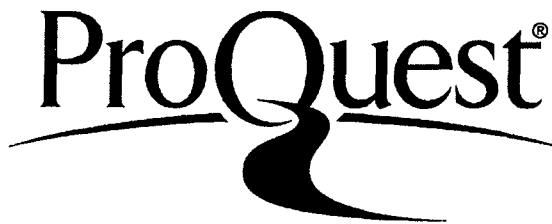
In the unlikely event that the author did not send a complete manuscript and there are missing pages, these will be noted. Also, if material had to be removed, a note will indicate the deletion.



UMI 1507833

Copyright 2012 by ProQuest LLC.

All rights reserved. This edition of the work is protected against unauthorized copying under Title 17, United States Code.

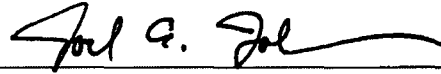


ProQuest LLC  
789 East Eisenhower Parkway  
P.O. Box 1346  
Ann Arbor, MI 48106-1346

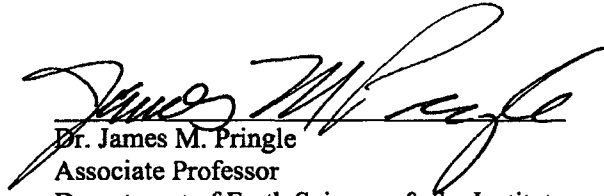
This thesis has been examined and approved.



Thesis Advisor, Dr. Rosemarie E. Came  
Assistant Professor of Climate Science  
Department of Earth Sciences



Dr. Joel E. Johnson  
Associate Professor of Geology  
Department of Earth Sciences



Dr. James M. Pringle  
Associate Professor  
Department of Earth Sciences & the Institute  
for the Study of Earth, Ocean and Space

1 December 2011  
Date

*This work is dedicated to my husband, parents, family and friends.*

## ACKNOWLEDGEMENTS

I would like to thank everyone who helped me along the path that has led to the completion of this thesis.

First, I would like to thank Rose Came, who has been a wonderful advisor, mentor and friend through this process. I followed her halfway across the country and have never regretted the decision. Dr. Came helped me out of a dark place in my first semester of graduate school and has been a constant source of support since.

I would like to thank my committee members, Dr. Joel Johnson and Dr. Jamie Pringle, for their support and assistance. I appreciate the guidance they each provided and the time they took to help me along the way towards completing my thesis. Many thanks go out to Dr. Joel Johnson, Dr. Liviu Giosan and the shipboard science party and crew from the NGHP-01 cruise for their hard work and dedication in collecting the sediment cores that made this research possible.

An encompassing thanks goes out to all faculty and staff both at UNH and UT for helping me navigate the murky waters of graduate school and for teaching me things I never thought possible and helping me to understand how this world works, literally and figuratively.

I would like to send special thanks out to my friends at the Woods Hole Oceanographic Institution. Going to sea with that special group of people three times in one year was a gift I never could have seen coming and will always look back on fondly. I would like to express my sincerest gratitude to Dr. Delia Oppo at Woods Hole Oceanographic Institution for the use of her clean lab facility for sample preparation.

To all of the friends I have made within the confines of these academic walls, thank you for always lending an ear when things needed to be said rather than thought and for helping me to reason through things when a wall popped up.

Thank you to each of the professors for whom I was a teaching assistant. The skills

and experiences I gained through each semester of teaching are innumerable. I honestly feel that I never learned more effectively than when I needed to prepare to teach something that was vaguely known to me or, at times, completely unknown.

My husband, Michael, supported me through this entire experience and without the constancy of that support, I may have faltered. My parents have never once doubted me and have always been supportive of my choices and for that, I thank them. Thank you to the rest of my family for always being proud of me and supporting me.

This work was funded by the support of two years of UNH Department of Earth Sciences Teaching Assistantships, the Karen Von Damm Memorial Scholarship, the ESCI-EOS Student Research Fund, the NRESS Student Support Fund, the UNH Graduate School Summer Teaching Assistant Fellowship, the generosity of the NOSAMS laboratory, the NGHP-01 post-cruise research funds of Dr. Joel Johnson, and the start-up funds of Dr. Rosemarie Came.

## TABLE OF CONTENTS

DEDICATION .....	iii
ACKNOWLEDGEMENTS .....	iv
LIST OF TABLES .....	vii
LIST OF FIGURES .....	viii
ABSTRACT .....	ix

CHAPTER	PAGE
1. INTRODUCTION .....	1
2. STUDY AREA .....	5
3. MATERIALS AND METHODS .....	11
4. RESULTS .....	16
5. DISCUSSION .....	18
6. CONCLUSION .....	27
LIST OF REFERENCES .....	29
APPENDIX A: TABLES .....	34
APPENDIX B: PICTURES .....	45



## LIST OF TABLES

Table 1 – Radiocarbon Data .....	35
Table 2 – Foraminiferal Data .....	36
Table 3 – Foraminiferal Mg/Ca Data .....	38
Table 4 – Foraminiferal $\delta^{18}\text{O}$ Data .....	40
Table 5 – Residual Seawater $\delta^{18}\text{O}$ Data .....	43

## LIST OF FIGURES

Figure 1 – Map of study area .....	5
Figure 2 – Annual temperature contour map of the Bay of Bengal .....	6
Figure 3 – Seasonal salinity contour maps of the Bay of Bengal .....	8
Figure 4 – Seasonal surface current maps of the Bay of Bengal .....	9
Figure 5 – Results versus depth .....	17
Figure 6 – Planktic foraminiferal data versus age .....	19
Figure 7 – Comparison of regional records .....	22
Figure 8 – June, July, August averaged surface currents in the Bay of Bengal .....	23

ABSTRACT

RECONSTRUCTING THE VARIABILITY IN THE INDIAN MONSOON  
FROM THE LAST GLACIAL PERIOD TO PRESENT

By

Sarah Schulenberg

University of New Hampshire, December 2011

Asian monsoon rains provide freshwater to one of the most densely populated regions on Earth. However, despite the societal and economic importance of the monsoon, its forcing mechanisms are not fully understood. Here I present a new reconstruction of monsoon variability from the last glacial period to the present as recorded in planktic foraminiferal Mg/Ca and  $\delta^{18}\text{O}$  of a marine sediment core from the Mahanadi Basin in the northwestern Bay of Bengal.

This new reconstruction reveals an increase in the intensity of the summer monsoon since the last glacial period, in agreement with known changes in northern hemisphere summer insolation. Furthermore, it suggests that the intertropical convergence zone migrated northward during the Bølling-Allerød warm period, but not northward enough to impact the waters of the Mahanadi Basin.

## CHAPTER 1

### INTRODUCTION

The Asian Monsoon is the largest monsoon system on Earth. The water that falls as monsoon precipitation over Asia and India plays a major economic and societal role, supplying one of the most densely populated regions of the world with fresh water and hydration for crops. The Asian summer monsoon occurs as the result of the intense summer heating of Asian landmasses, which causes a large temperature gradient between the land and the nearby ocean. The temperature rise of the landmass causes the warmer, less dense air above the land to rise leaving behind a cell of low pressure. The intense summer heating of the Indian subcontinent also pulls the Intertropical Convergence Zone (ITCZ) northward seasonally. The presence of this low-pressure cell combined with the shift in the position of the ITCZ drives southwest monsoon winds bringing moist, cooler air in from the ocean. This, in turn, causes greater amounts of precipitation over land than those seen during the winter monsoon season when the system is reversed.

The strength of the Asian summer monsoon is hypothesized to vary on annual to decadal timescales due to factors such as the state of the El Niño-Southern Oscillation (ENSO) [*Schott and McCreary, 2001*], changes in Tibetan Plateau snow cover [*Barnett et al., 1988*], and the migration of the mean annual position of the ITCZ [*Haug et al., 2001*]. In addition, it is widely accepted that the intensity of the Asian monsoon has varied in response to changes in the Earth's orbital parameters, with increases in northern hemisphere (NH) summer insolation causing increases in the intensity of the monsoon response [*Kutzbach, 1981; Prell and Kutzbach, 1987*]. The amount of insolation received

by mid to low latitudes changes with the precession of the equinoxes on a cycle of approximately 23,000 years, as described by Milankovitch (and separately by Croll) [Milankovitch, 1941; Croll, 1875]. It stands to reason that an increase in the summer insolation received by the Asian landmass at mid to low latitudes would lead to a stronger temperature gradient being established between land and ocean creating an enhanced summer monsoon response. Conversely, when incoming summer insolation is lower, a weaker temperature gradient would be established between land and ocean and a weaker monsoon response would be expected.

The results of previous paleoclimate studies largely support the hypothesis that orbital parameters influence the intensity of the summer monsoon [Cheng *et al.*, 2006; Wang *et al.*, 2001, 2005, 2008; Clemens *et al.*, 1991, 2003, 2007; Overpeck *et al.*, 1996; Dykoski *et al.*, 2005; Kudrass *et al.*, 2001; Rashid *et al.*, 2007, 2011; Altabet *et al.*, 2002; etc.]. However, paleoclimate archives from the areas affected by the Asian monsoon yield conflicting evidence about the timing of the monsoonal response with respect to NH insolation changes. In China, variability in the strength of the Asian Monsoon has been reconstructed using the oxygen isotopic composition ( $\delta^{18}\text{O}$ ) of speleothem calcite [Cheng *et al.*, 2006; Wang *et al.*, 2001, 2005, 2008]. These studies reveal long-term  $\delta^{18}\text{O}$  trends that follow the record of NH summer insolation, suggesting no lag between changes in NH insolation and changes in monsoon strength. The records also exhibit changes on sub-orbital timescales that appear to be synchronous with the sub-orbital scale variability recorded in Greenland ice.

Marine sediment cores from the Arabian Sea have also been used to study the variability in the strength of the Asian monsoon. Multi-proxy data (biogenic opal flux, the abundance of *Globigerina bulloides*, excess barium flux and lithogenic grain size) from Arabian Sea sediment cores have been used to reconstruct monsoon variability over the past 350,000 years [Clemens *et al.*, 1991, 2003]. The authors found that their monsoon records were dominated by precession bands, and by obliquity bands on much longer

timescales. However, the authors found that the maxima in the strength of the monsoon lagged the peak in NH summer insolation by approximately 8,000 years. Similarly, reconstructions using pollen counts and percent abundances of *G. bulloides* in other Arabian Sea sediment cores yield comparable results, with monsoon intensity lagging peak summer insolation by 3,000 years [Overpeck *et al.*, 1996].

The reason for the disagreement between the reconstructions using the  $\delta^{18}\text{O}$  of Chinese cave deposits and the reconstructions using Arabian Sea marine sediment cores is not known. One explanation is that Chinese speleothem calcite does not provide a record of monsoon variability, but rather, it records environmental changes in the Pacific Ocean where precipitation source waters originate [Clemens *et al.*, 2007]. However, the agreement between the  $\delta^{18}\text{O}$  records from Chinese speleothems located within both the East Asian [Wang *et al.*, 2001, 2008] and Indian monsoon [Dykoski *et al.*, 2005] regions suggests that speleothem  $\delta^{18}\text{O}$  reconstructions may be representative of the overall Asian monsoon and are not under strong regional controls. Alternatively, the paleoclimate reconstructions from the Arabian Sea and from eastern China may both represent true monsoon signals, with India and China having very different climatic responses to NH summer insolation, suggesting a complex relationship between insolation forcing and the climatic response of the monsoon system. The Bay of Bengal, which lies geographically between the Arabian Sea and eastern China, is an ideal place to reconstruct past conditions in an attempt to resolve this disagreement. Unlike precipitation over eastern China, precipitation over the Bay of Bengal originates in the Indian Ocean, not the Pacific.

The Bay of Bengal, which receives most of its freshwater input during the summer monsoon months, is an ideal location to investigate monsoonal variability. However, very few records of monsoon variability have been generated within the Bay. Monsoon intensity was reconstructed using  $\delta^{18}\text{O}$  of *Globigerinoides ruber* and alkenone-derived temperatures in the northernmost Bay of Bengal [Kudrass *et al.*, 2001]. In this study, the

authors concluded that feedback processes involving snow and dust cover of the Tibetan Plateau primarily control the variations in the intensity of the summer monsoon. More recently, paired records of foraminiferal Mg/Ca and  $\delta^{18}\text{O}$  have been generated using sediment cores from the Andaman Sea [Rashid *et al.*, 2007] and southwestern Bay of Bengal [Rashid *et al.*, 2011]. These records reveal geographic variations in the monsoon response within the Bay of Bengal, lending yet more uncertainty into the overall forcing and regional response of the monsoon.

In this study, I present 22,000-year records of paired planktic foraminiferal magnesium-to-calcium ratios (Mg/Ca) and  $\delta^{18}\text{O}$ , which were generated using a sediment core retrieved from the Mahanadi Basin in the northwestern Bay of Bengal. The  $\delta^{18}\text{O}$  of planktic foraminiferal tests is commonly used as an indicator of sea surface salinity [e.g. Bond *et al.*, 1993]. However, carbonate  $\delta^{18}\text{O}$  ( $\delta^{18}\text{O}_\text{C}$ ) is a function of both the calcification temperature and the  $\delta^{18}\text{O}$  of the seawater ( $\delta^{18}\text{O}_\text{sw}$ ) in which the carbonate grew. The Mg/Ca in the crystal lattice of a foraminiferal test has been shown to be temperature dependent [Nürnberg *et al.*, 1996]. Therefore, by using the two methods of  $\delta^{18}\text{O}_\text{C}$  and Mg/Ca in concert, it is possible to isolate the  $\delta^{18}\text{O}_\text{sw}$ , which co-varies with salinity. The timing and intensity of the  $\delta^{18}\text{O}_\text{sw}$  variations as recorded in the Mahanadi Basin sediment core are compared with the timing and intensity of variations recorded in other sediment cores from the Bay of Bengal [e.g. Rashid *et al.*, 2007, 2011]. In addition, the new record is interpreted in light of known changes in NH summer insolation and within the context of previously published paleoclimate archives from the entire Asian monsoon region.

## CHAPTER 2

### STUDY AREA

#### *Core Description*

The marine sediment core used in this study was retrieved during the first expedition of the Indian National Gas Hydrate Program [Collett *et al.*, 2008]. Core site NGHP-01-19 in the Mahanadi Basin ( $18^{\circ} 58.6568'N$ ,  $85^{\circ} 39.5202'E$ , 1,433.2 meters depth) (Figure 1) was originally selected to investigate the area for the presence or absence of gas hydrates. Two cores were collected at the site: 19A and 19B. The portion of NGHP-01-19B used

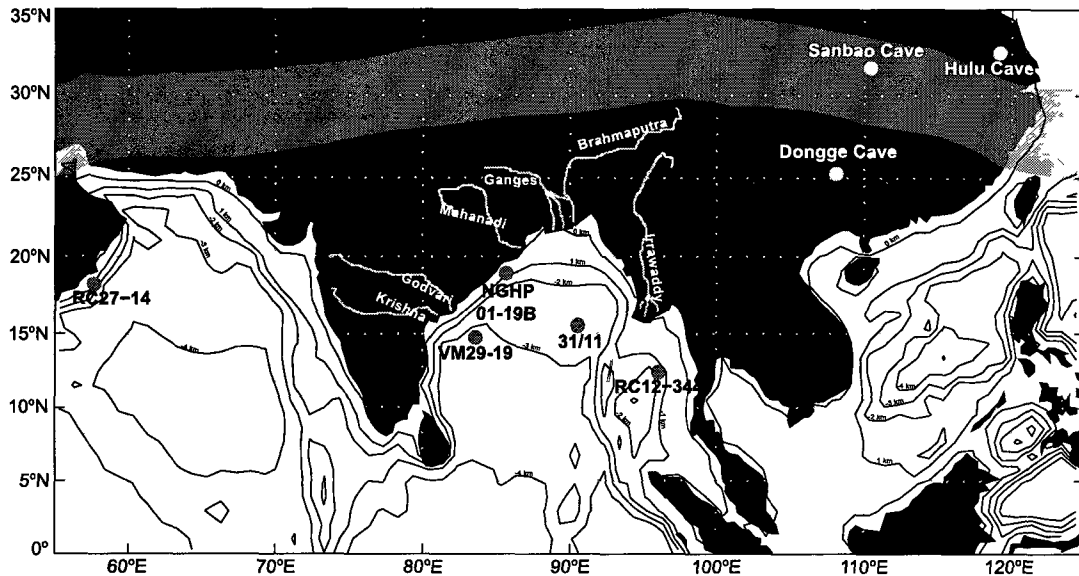


Figure 1. Map of the study area showing the locations of NGHP-01-19B ( $18^{\circ}58.7'N$ ,  $85^{\circ}39.5'E$ , 1,433 m), 31/11 ( $15^{\circ}52.0'N$ ,  $91^{\circ}10.0'E$ , 2,713 m) [Chauhan, 2003], VM29-19 ( $14^{\circ}42.6'N$ ,  $83^{\circ}34.8'E$ , 3,182 m) [Rashid *et al.*, 2011], RC12-344 ( $12^{\circ}27.6'N$ ,  $96^{\circ}24'E$ , 2,140 m) [Rashid *et al.*, 2007], RC27-14 ( $18^{\circ}15.2'N$ ,  $57^{\circ}39.3'E$ , 596 m) [Altabet *et al.*, 2002], Hulu Cave ( $32^{\circ}30'N$ ,  $119^{\circ}10'E$ ) [Wang *et al.*, 2001], Sanbao Cave ( $31^{\circ}40'N$ ,  $110^{\circ}26'E$ ) [Wang *et al.*, 2008], and Dongge Cave ( $25^{\circ}17'N$ ,  $108^{\circ}5'E$ ) [Dykoski *et al.*, 2005]. The red swath represents the modern northern extent of the ITCZ. Black contours indicate bathymetry labeled in kilometers below sea level.



for this study lies above the depth at which gas hydrates were found [Collett *et al.*, 2008] and, therefore, it is unlikely that diagenesis associated with methane and/or gas hydrates affects our data interpretation and analysis. NGHP-01-19B consists of three segments, yielding a total length of 26.3 meters, which were retrieved by means of advanced piston core [Collett *et al.*, 2008].

#### *Water Balance of the Bay of Bengal*

Varkey *et al.* [1996] present the most comprehensive report of the modern hydrological conditions within the Bay of Bengal, which is dominated by freshwater input from the massive river systems that feed into it (Figure 1). The authors report the

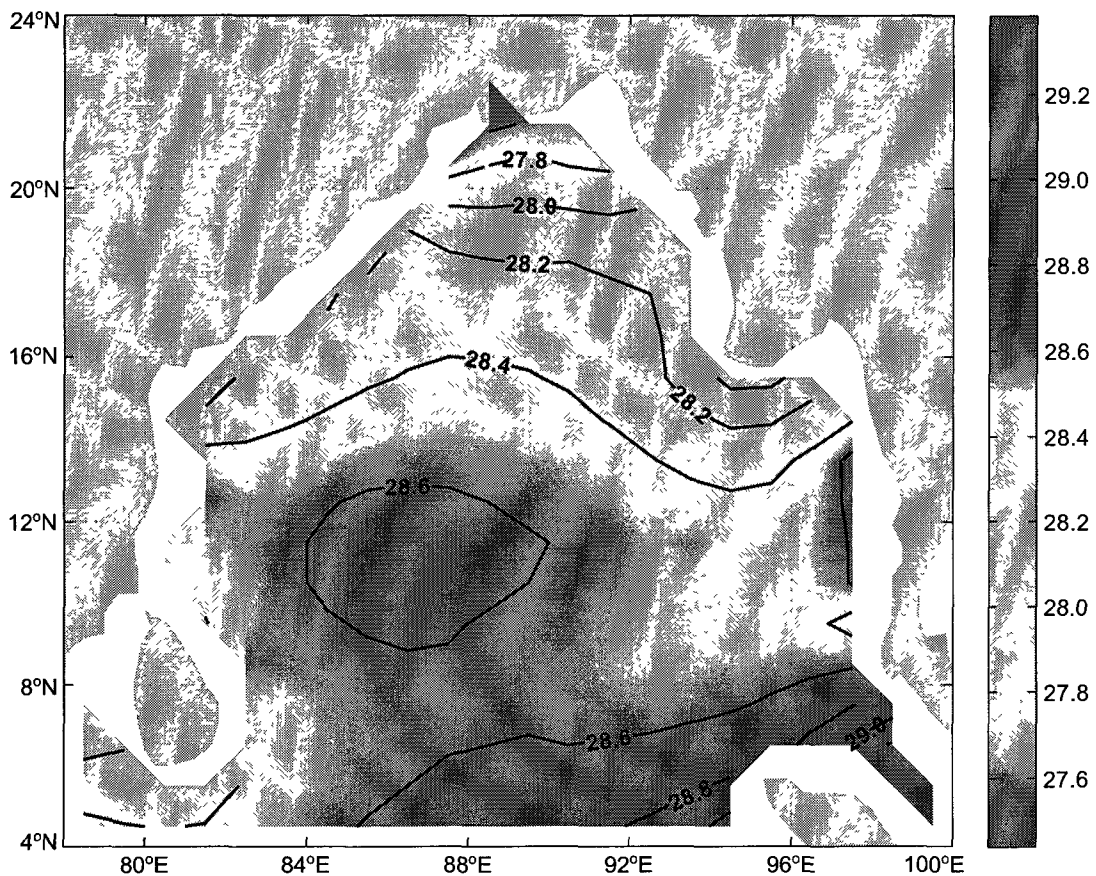


Figure 2. Map of Bay of Bengal showing mean annual sea surface (0 m) temperatures. Data from World Ocean Atlas (WOA) 2005 [Locarnini *et al.*, 2006].

total yearly runoff received by the Bay from Myanmar (Burma), Bangladesh and the east coast of India to be estimated at 2,125 km<sup>3</sup> or approximately 0.05 to 0.06 Sv (1 Sv = 10<sup>6</sup> m<sup>3</sup> s<sup>-1</sup>). The authors also report that the net water exchange, taking into account evaporation, runoff and precipitation, within the area encompassed by 15 - 20°N latitude and 80 - 90°E works out to a net loss during the winter monsoon months (December, January and February) of -93.41 km<sup>3</sup> and a net gain of 209.80 km<sup>3</sup> during the summer monsoon months.

### *Surface Water Conditions*

Annual surface temperatures within the central Bay of Bengal vary between 27 and 29°C; higher temperature gradients are seen along the coast lines and the coolest surface temperatures are seen near the rivers with the largest annual runoff: the Ganges-Brahmaputra river system in the north central Bay (~27.5°C) and the Irrawaddy River in the eastern Bay (~27.6 to 27.7°C) (Figure 2) [Locarnini *et al.*, 2006]. The coolest surface temperatures are observed in the Bay during the summer monsoon months with slightly cooler temperatures also observed during the winter monsoon months. During the transition periods between monsoon seasons, warm water penetrates back into the Bay [Locarnini *et al.*, 2006].

Salinity in the Bay of Bengal ranges from approximately 27 to 35 annually (Figure 3) [Antonov *et al.*, 2006]. Salinity levels in the Bay are lowest near the rivers with the largest annual runoff, similar to the temperature pattern. During the months of the summer monsoon and into the transition period towards winter monsoon conditions, the lowest salinity levels migrate east from the Mahanadi Basin to the mouth of the Irrawaddy River. During the winter monsoon months low salinity levels migrate farther into the center of the Bay due to the growing difference in evaporation versus precipitation [Antonov *et al.*, 2006].

The currents in the Bay of Bengal shift seasonally (Figure 4) [Lumpkin and Garraffo,

2005] in response to seasonally shifting winds [Schott *et al.*, 2009]. During the oceanic winter, surface currents travel northward along the western boundary over the Mahanadi Basin with southward return flow to the east. A small gyre with southward currents along the western boundary is established in the northern Bay during the spring months while the rest of the Bay remains dominated by northward flowing western boundary currents. In the oceanic summer, the gyre in the northern Bay extends farther south, fully encompassing the Mahanadi Basin and converging with northward flowing western boundary currents at approximately 16°N. During the oceanic fall, the system reverses with waters moving southward along the western boundary.

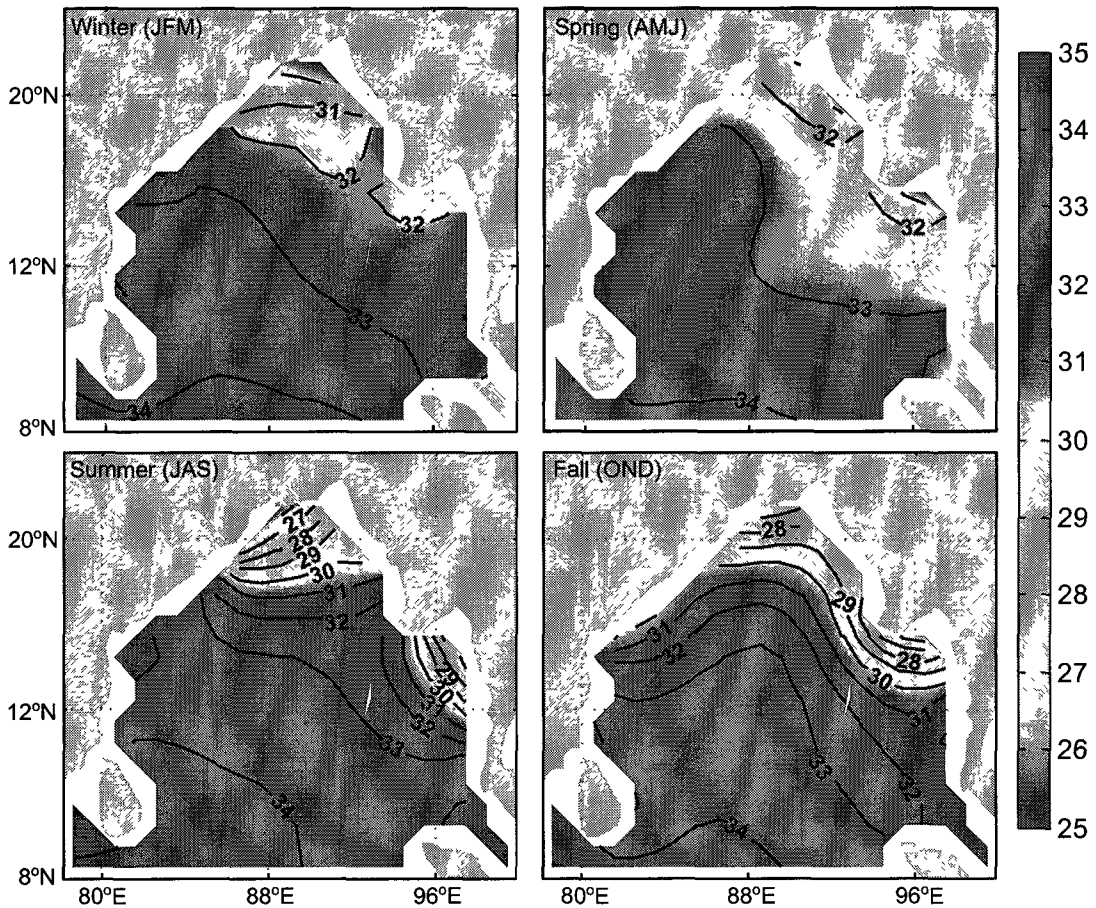


Figure 3. Maps of Bay of Bengal showing mean seasonal surface (0 m) salinity. Data from World Ocean Atlas (WOA) 2005 [Antonov *et al.*, 2006].

## Upwelling and Downwelling

Wind-driven upwelling also impacts surface conditions in the Bay of Bengal. Strong upwelling during the summer monsoon and strong downwelling during the winter monsoon were found by *Varkey et al.*, [1996] after the calculation of an upwelling index (UI) at eight stations along the east coast of India. The seasonal shift between upwelling and downwelling is attributed to the seasonally shifting winds caused by the annually migrating ITCZ. Upwelling during the summer monsoon brings cooler, more saline waters towards the surface. The strength of upwelling along the east coast of India has been found to have a lag response to the ENSO index in the Pacific [*Krishna and Rao*,

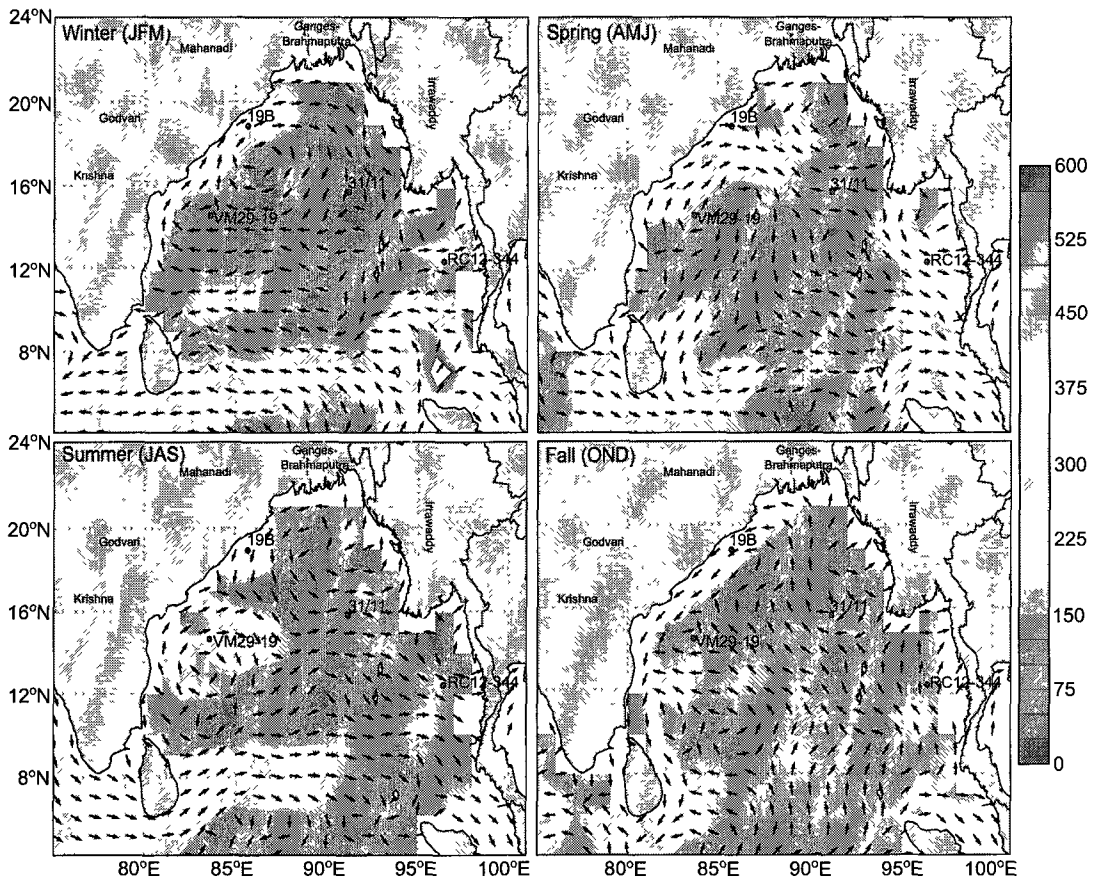


Figure 4. Maps of Bay of Bengal showing seasonal averaged surface (0 m) currents in km per 10 days [Lumpkin and Garraffo, 2005] with circles indicating the locations of NGHP-01-19B, 31/11 [Chauhan, 2003], and VM29-19 [Rashid et al., 2011], RC12-344 [Rashid et al., 2007]. Blue lines indicate approximate locations of major rivers feeding into the Bay.

2009]. These authors showed that wind fluctuations off the east coast of India were coherent with fluctuations in the Pacific Ocean ENSO index. With more intense offshore winds, coastal upwelling is strengthened and more cold, saline, nutrient-rich water is brought to the surface from depth, increasing productivity.

### *Subsurface Water Masses*

The contributions of various subsurface water masses to the Bay of Bengal are not well constrained. Intermediate waters of the Bay have been attributed to three major source water masses: Antarctic Intermediate Water (AAIW) from the south, Indonesian Intermediate Water (IIW) from the east and Red Sea Intermediate Water (RSIW) including the influence of waters from the Persian Gulf from the west [You, 1998]. At greater depths (below 1500 m), a cool, high salinity, low-oxygen water mass, Northern Indian Deep Water, which is itself a mixture of Arabian Sea Intermediate Water and Indian Ocean Bottom Water, penetrates the Bay. Antarctic Bottom Water may also be present in the deepest parts of the Bay [Varkey *et al.*, 1996].

## CHAPTER 3

### MATERIALS AND METHODS

#### *Radiocarbon Dating*

The age model for site NGHP-01-19 was developed using five accelerator mass spectrometer (AMS) radiocarbon dates: four from NGHP-01-19B and one from NGHP-01-19A, the companion core extracted 10 m from NGHP-01-19B. The NGHP-01-19B-specific age model was developed by adjusting the depth interval for the radiocarbon sample taken from NGHP-01-19A by 3.8 cm based on a comparison of magnetic susceptibility records of both cores [Collett *et al.*, 2008]. The foraminiferal samples used for dating were picked from all size fractions >150  $\mu\text{m}$  and consisted of mixed planktic foraminifera for the core top and NGHP-01-19A samples, mixed *G. ruber* and *G. sacculifer* for the 194-195 cm sample, and *G. ruber* only for the 258-259 cm and 354-355 cm samples. Radiocarbon analyses were performed by the National Ocean Sciences Accelerator Mass Spectrometer (NOSAMS) Facility at the Woods Hole Oceanographic Institution. Radiocarbon dates were converted to calendar years before present (1950) using CALIB 6.0 [Stuiver and Reimer, 1993], the Marine09 calibration dataset [Reimer *et al.*, 2009] and the standard reservoir correction of 400 years applied by the CALIB 6.0 algorithm. No additional reservoir age correction was applied after determining that the available  $\Delta R$  values for the region [Dutta *et al.*, 2001; Southon *et al.*, 2002] would not prove significant on the timescales examined in this study. The ages used in the model were determined by taking the median age of the 1-sigma age range with the highest probability as reported by CALIB 6.0. Each sample depth interval was then converted to

calendar years BP in kyr using linear interpolation, assuming constant sedimentation rates between the radiocarbon dates converted to calendar ages.

### *Sample Preparation*

Sediment samples for Mg/Ca and stable isotope analyses were collected from core NGHP-01-19B, which is housed at the Woods Hole Oceanographic Institution Core Repository. Initially, the samples consisted of 1-by-2.5 cm blocks of sediment, and were collected every 8 cm from 8 to 370 cm below the sea floor (cmbsf). However, because the sedimentation rate was lower in the deeper portion of the core, the core was later sub-sampled at 4 cm spacing from 210 to 322 cmbsf in order to improve the time resolution. Conversely, because the sedimentation rate was high in the upper portion of the core, foraminiferal abundances were low. In order to acquire adequate foraminiferal material, all samples in the upper 244 cm of the core were increased in size by sampling the 1 cm of sediment just below the initial sample. Samples were brought back to the University of New Hampshire, to be frozen and freeze-dried for approximately 24 hours. The freeze-dried samples were rinsed with warm, soft-pressure tap water in 63  $\mu\text{m}$  sieves to remove the clay and silt fractions before being dried in a 50°C oven for at least two to three hours. This process was repeated a total of five times for all samples before they were transferred to glass, screw top vials.

*G. ruber* (white) tests of high visual quality (See pictures in Appendix B) were picked from the 212-250  $\mu\text{m}$  size fraction when abundances allowed and additionally from the 250-300  $\mu\text{m}$  size fraction if abundances were low. The species *G. ruber* is one of the eight foraminiferal species that dominate the foraminiferal population in the Bay of Bengal. *G. ruber*, in particular, is abundant in the northern Bay of Bengal, the region from which the core was retrieved [Guptha et al., 1997]. Based on sediment trap data, *G. ruber* reaches an abundance maximum during the summer monsoon [Guptha et al., 1997], which makes it ideal for tracking the strength of the summer monsoon because

the tests of foraminifera record the conditions under which they grow. When abundances allowed, 100 individual *G. ruber* (white) tests were picked from each sediment sample; however, at times, fewer than 10 individuals were present. Each group of picked individuals was gently crushed between two glass microscope slides in order to open the chambers for cleaning. Each crushed foraminiferal sample was then homogenized and split into separate aliquots for Mg/Ca and  $\delta^{18}\text{O}_c$  analyses. Each Mg/Ca aliquot consisted of a mass of calcite that was equivalent to approximately 30 to 40 individual tests (but ranging to as low as 6 individuals) and each  $\delta^{18}\text{O}_c$  aliquot consisted of a mass that was equivalent to approximately 4 to 10 individuals.

#### *Geochemical Analyses*

Mg/Ca samples were cleaned using the full trace metal method of *Boyle and Keigwin* [1985/6] with the oxidative and reductive steps reversed [*Rosenthal et al.*, 1999]. Cleaned, high-carbonate samples were dissolved with a volume of 0.5 N nitric acid that brought the solution to a calcium concentration of approximately 50 ppm and low-carbonate samples were dissolved to approximately 30 ppm. Mg/Ca data were generated on a Thermo-Finnegan Element2 sector field single collector inductively coupled mass spectrometer (ICP-MS) according to the protocol of *Rosenthal et al.* [1999]. Blanks and standards were run between every four samples for 50 ppm samples and between every three samples for the 30 ppm samples. The standard was 50 ppm when high-abundance samples were analyzed and 30 ppm when low-abundance samples were analyzed. In addition, in order to correct for any potential calcium matrix effect, the Mg/Ca standard was diluted and analyzed at varying calcium concentrations, which ranged from 10 ppm to 90 ppm. Three consistency standards were run at the start of the day to monitor the consistency of the instrument. The Mg/Ca values of the consistency standards measured  $1.65 \text{ mmol mol}^{-1}$ ,  $3.34 \text{ mmol mol}^{-1}$ , and  $4.99 \text{ mmol mol}^{-1}$ . Long-term standard deviations for these standards are  $\pm 0.04 \text{ mmol mol}^{-1}$  (n=24),  $\pm 0.09 \text{ mmol mol}^{-1}$  (n=22), and  $\pm 0.15$



mmol mol<sup>-1</sup> (n=22), respectively.

The ICP-MS intensity ratios were converted to Mg/Ca values in mmol mol<sup>-1</sup> after corrections for the blank, standard, and Ca matrix effects. The matrix corrections were less than ±0.00015 mmol mol<sup>-1</sup> Mg/Ca overall. Replicate foraminiferal samples were analyzed when abundances allowed. Average variance between replicates was ±0.022 mmol mol<sup>-1</sup>. The Mg/Ca values were converted to sea surface temperatures (SST) using the species-specific Mg/Ca-temperature relationship for *G. ruber* (white; 250-350 μm) of *Dekens et al.* [2002]:

$$\text{Mg/Ca (mmol mol}^{-1}\text{)} = 0.38 \exp [0.09 * \text{SST (}^{\circ}\text{C)}].$$

Stable isotope analyses were performed at the University of California Davis Stable Isotope Laboratory in the Department of Geology on a Fisons Optima isotope ratio mass spectrometer (IRMS) using an Isocarb common acid bath autocarbonate system at 90°C. Data are presented in the standard delta notation where:

$$\delta^{18}\text{O} = [(\text{R}_{\text{sample}}/\text{R}_{\text{standard}}) - 1] * 1000.$$

$\text{R}_{\text{sample}}$  and  $\text{R}_{\text{standard}}$  refer to the <sup>18</sup>O/<sup>16</sup>O ratios of the sample and reference standard, respectively. All δ<sup>18</sup>O<sub>C</sub> data are presented relative to Vienna Pee Dee Belemnite (VPDB). The analytical precision (± 1s) of the δ<sup>18</sup>O<sub>C</sub> data is ±0.06‰ based on repeat analyses of an in-house NBS-19 calcite standard.

The δ<sup>18</sup>O<sub>sw</sub> values were isolated from the δ<sup>18</sup>O<sub>C</sub> data using the Mg/Ca-derived SST and the *G. ruber* (white) temperature calibration equation of *Mulitza et al.* [2003]:

$$\text{SST (}^{\circ}\text{C)} = -4.44(\delta^{18}\text{O}_C - \delta^{18}\text{O}_{\text{sw}}) + 14.20.$$

The resulting δ<sup>18</sup>O<sub>sw</sub> values were adjusted by adding 0.27‰ so that δ<sup>18</sup>O<sub>sw</sub> is reported relative to Vienna Standard Mean Ocean Water (VSMOW). The effects of changes in global ice volume were corrected for with the relative sea level record of *Waelbroeck et al.* [2002] to arrive at the record of residual δ<sup>18</sup>O<sub>sw</sub> for core NGHP 01-19B. The equations of *Arbuszewski et al.* [2010] were not used to convert δ<sup>18</sup>O<sub>sw</sub> to salinity values in this study because that study focused on an Atlantic basin meridional transect that

experiences lower temperatures (16.7 – 27.6 °C) and higher salinities (35.48 – 37.28) than those observed in the Bay of Bengal.

## CHAPTER 4

### RESULTS

The AMS radiocarbon dates converted to calendar age yield an age model for core NGHP-01-19B with an increasing sedimentation rate from the deglaciation through to the core top (Figure 5, Panel a). The average sedimentation rate is  $\sim 17$  cm/kyr with lower values in the deeper portion of the core (4 cm/kyr) and higher values in the upper portion of the core (21 to 32 cm/kyr).

The Mg/Ca values in this core vary throughout, but reveal an overall increase of approximately  $0.8 \text{ mmol mol}^{-1}$  from the last glacial period to the present (Figure 5, Panel b). The minimum Mg/Ca value of  $3.58 \text{ mmol mol}^{-1}$  occurs at a depth of 354.5 cmbsf, which corresponds to a glacial age of 27.4 ka. The maximum Mg/Ca value of  $5.05 \text{ mmol mol}^{-1}$  occurs at a depth of 171 cmbsf, which corresponds to a Holocene age of 9.4 ka. The highest variability is seen between depths of 155 to 258.5 cmbsf, which correspond to pre- and early-Holocene ages (8.7 to 12.5 ka).

*G. ruber*  $\delta^{18}\text{O}_c$  shows a decrease of approximately 2‰ from the last glacial to the present (Figure 5, Panel c). The maximum in  $\delta^{18}\text{O}_c$  of -0.8‰ occurs at a depth of 298.5 cmbsf, which corresponds to an age of 16.7 ka. The Holocene  $\delta^{18}\text{O}_c$  has an average value of approximately -3‰. The record exhibits high variability between 171 and 235 cmbsf, which correspond to 9.4 and 11.8 ka respectively. There is an anomalously high value of -1.6‰ occurring at 219 cmbsf (11.3 ka).

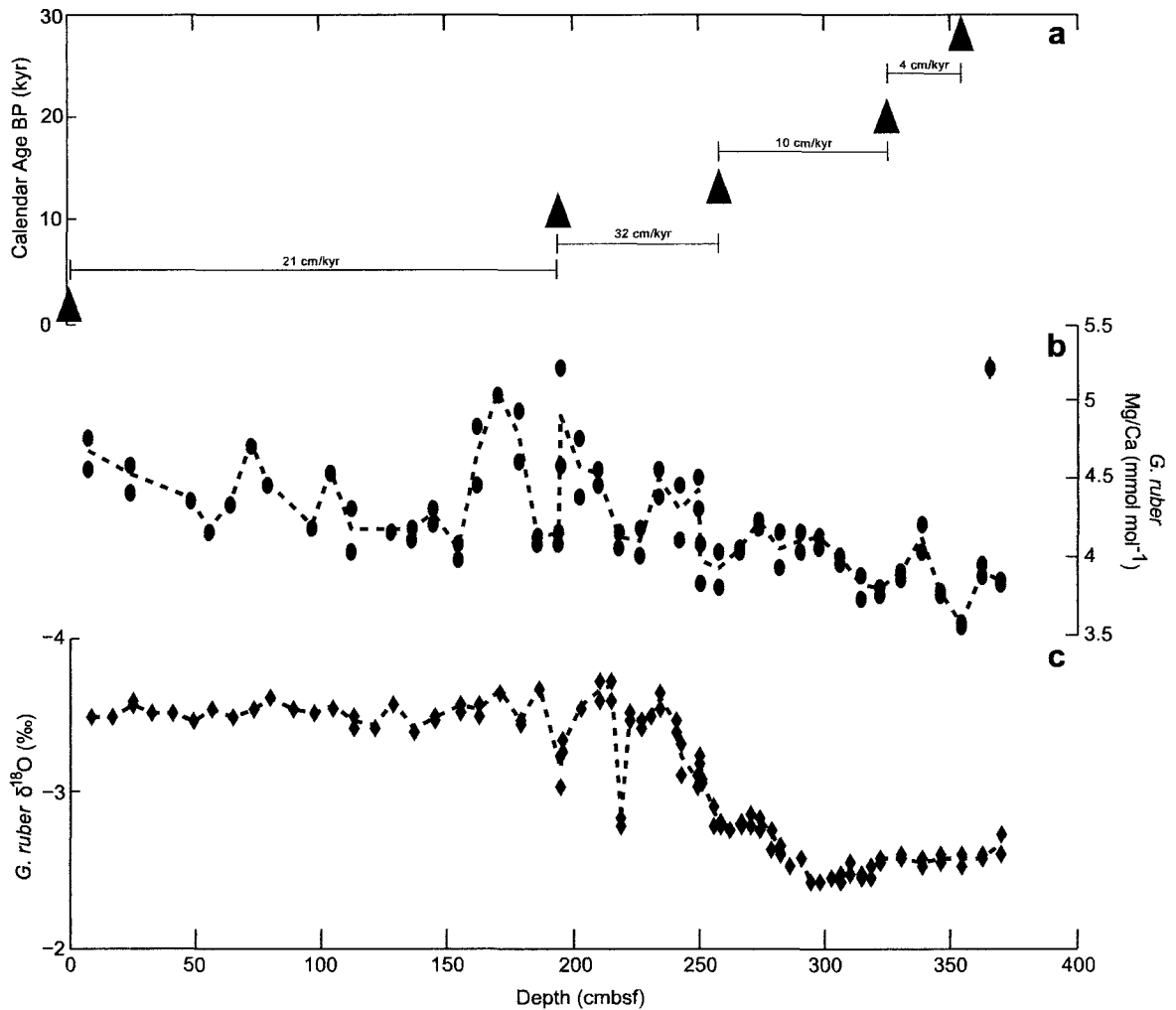


Figure 5. Planktic foraminiferal data from NGHP-01-19B vs. depth. (a) Median 1-sigma accelerator mass spectrometer (AMS) radiocarbon dates converted to calendar age (black triangles). Errors bars on each datum are smaller than the plotted symbol. Labeled bars illustrate linearly interpolated sedimentation rates. (b) All *G. ruber* Mg/Ca data (red circles), with average Mg/Ca where replicates exist (dashed red line). Maximum analytical error plotted in upper right hand corner (red circle with bar). (c) All *G. ruber* δ<sup>18</sup>O data (blue diamonds), with average δ<sup>18</sup>O where replicates exist (dashed blue line). Error bar is smaller than symbol. Both data sets were passed through a 3-standard deviation filter to ensure statistical significance.

## CHAPTER 5

### DISCUSSION

Results from NGHP-01-19B reveal an overall trend of increasing SST from the last glacial period to the present, with the lowest temperature of 24.9°C occurring at 27.4 ka and the highest temperature of 28.8°C occurring at 9.4 ka (Figure 6, Panel d). A period of highly variable temperature occurred between 12.5 and 8.7 kyrs before present. The core-top temperature of 27.9°C at 1.8 ka falls within the present temperature range observed at the study site (Figure 2) [Locarnini *et al.*, 2006].

The  $\delta^{18}\text{O}_{\text{sw}}$  at the core site decreased by approximately 1‰ from the average value of the last glacial to the average value of the Holocene (Figure 6, Panel e), suggesting an intensification of the Indian monsoon over this time period. The maximum  $\delta^{18}\text{O}_{\text{sw}}$  value of 1.3‰ occurred at 16.7 ka and the minimum  $\delta^{18}\text{O}_{\text{sw}}$  value of -0.42‰ occurred at 10.2 ka. As with the SST record, there is high variability in  $\delta^{18}\text{O}_{\text{sw}}$  between 12.5 and 8.7 kyrs before present. The presence of high variability in both Mg/Ca and  $\delta^{18}\text{O}_{\text{c}}$  between 12.5 and 8.7 kyrs before present (Figure 5, Panels b and c) suggests that the variability in the derived  $\delta^{18}\text{O}_{\text{sw}}$  is likely not an instrumental artifact. The core-top  $\delta^{18}\text{O}_{\text{sw}}$  at 1.8 ka of 0.4‰ is similar to modern values of 0 – 0.5‰ [Delaygue *et al.*, 2001].

The minimum in  $\delta^{18}\text{O}_{\text{sw}}$  recorded in the Mahanadi Basin, which may be inferred as the peak in monsoon strength, occurred near the peak in summer insolation at 30°N (Figure 6, Panel a) [Berger and Loutre, 1991] but may have lagged it by approximately one or two thousand years. The overall trend appears to be in phase with the GISP2  $\delta^{18}\text{O}$  record (Figure 6, Panel b) [Grootes and Stuiver, 1999] as well as the Vostok  $\delta\text{D}$  record

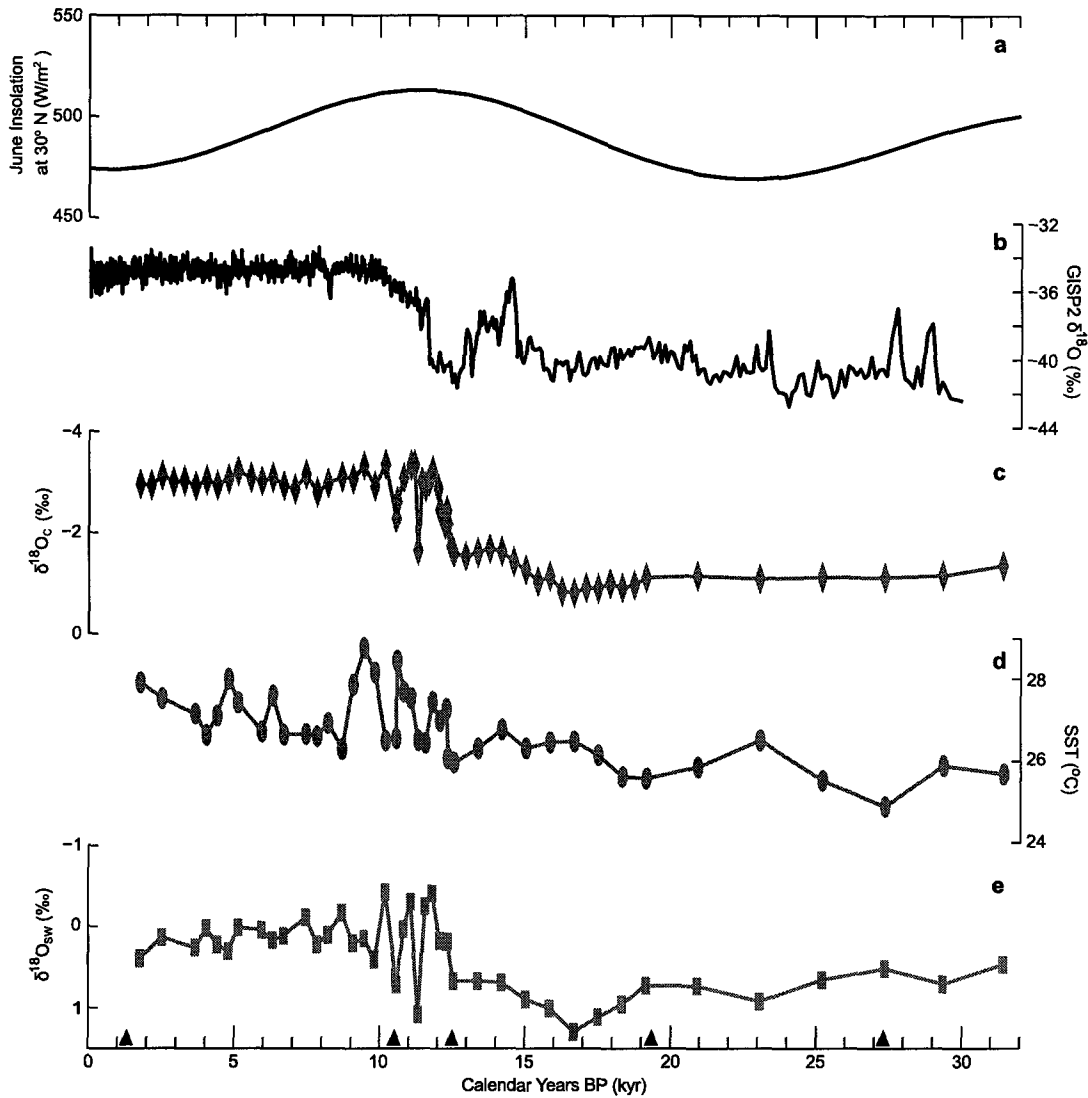


Figure 6. Planktic foraminiferal data from NGHP-01-19B vs. age. (a) June insolation at 30°N (black line) [Berger and Loutre, 1991]. (b) GISP2  $\delta^{18}\text{O}$  [Grootes and Stuiver, 1999] (black line). (c) Average *G. ruber*  $\delta^{18}\text{O}$  (blue diamonds, blue line). (d) Average Mg/Ca-derived SST (red circles, red line). (e) *G. ruber* residual  $\delta^{18}\text{OSW}$  (magenta squares, magenta line). Black triangles indicate radiocarbon dates converted to calendar ages.

(Figure 7, Panel i) [Petit et al., 2001], coming out of the last glacial period starting at approximately 16 ka and reaching Holocene values by approximately 9 ka.

#### *Comparison to other Bay of Bengal records*

There are few reconstructions of sea surface temperature and surface water conditions in or near the Bay of Bengal. The records that do exist [Chauhan, 2003; Rashid et al., 2007, 2011] (Figure 1) exhibit differences among one another and in comparison to the NGHP-01-19B records. *G. ruber*-derived Mg/Ca results from core RC12-344 from the Andaman Sea [Rashid et al., 2007] and from core VM29-19 from the southwestern Bay of Bengal [Rashid et al., 2011] reveal temperature shifts from the last glacial period to the Holocene of approximately 2.4°C and 2.8°C, respectively. These shifts are somewhat larger than the 1.4°C temperature shift from the average of the last glacial to the core top recorded in the Mahanadi Basin (Figure 6, Panel d).

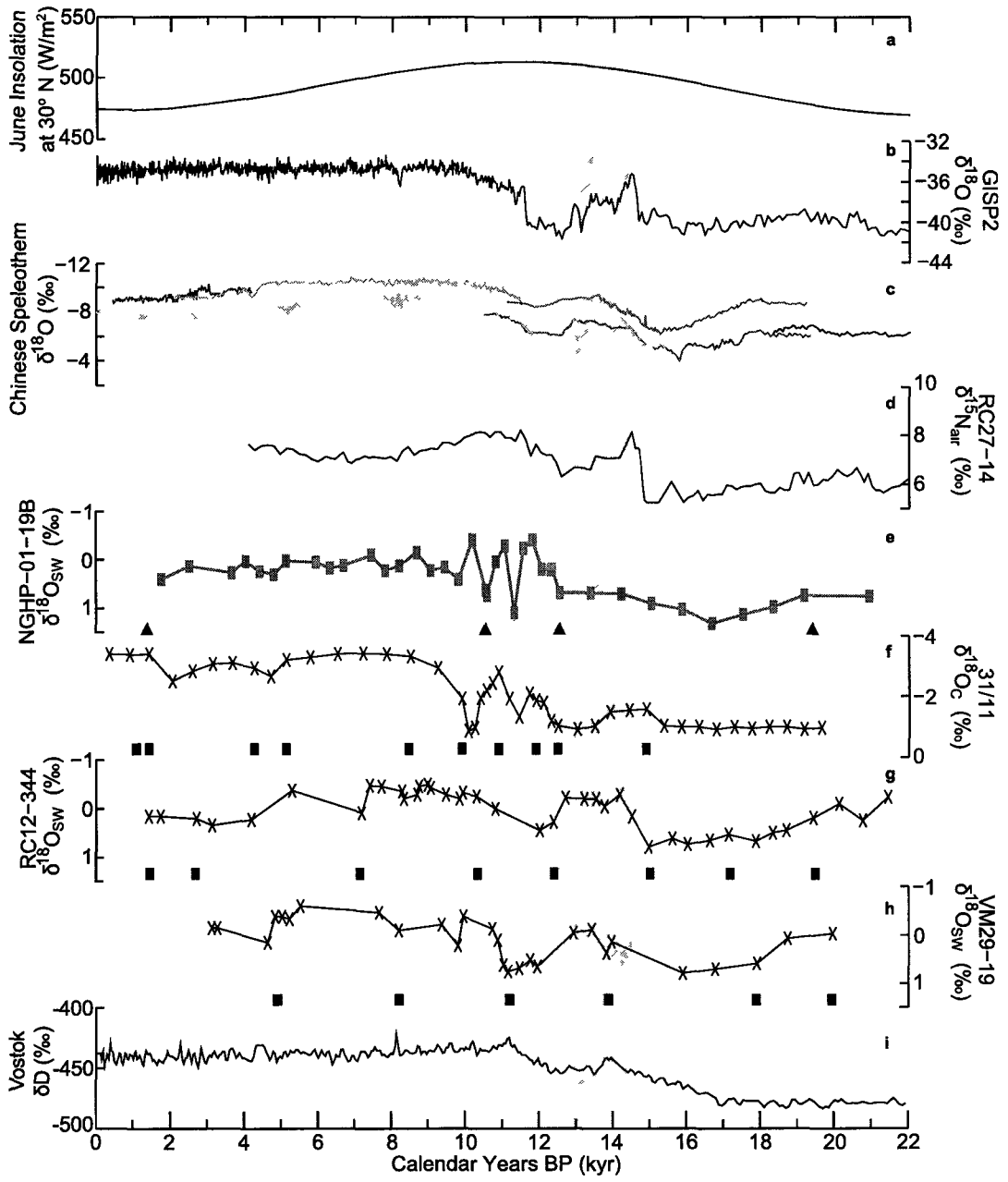
The glacial to interglacial trend in the NGHP-01-19B  $\delta^{18}\text{O}_{\text{sw}}$  reconstruction is similar to those from the Andaman Sea (RC12-344) and the southwestern Bay (VM29-19) [Rashid et al., 2007, 2011] in the marked decrease (or freshening, either due to increased river runoff or direct rainfall) of approximately 1‰ seen between the last glacial period and Holocene (Figure 7, Panels e, g and h).

During the Bølling-Allerød, the  $\delta^{18}\text{O}_{\text{sw}}$  values in the Andaman Sea and the southwestern Bay of Bengal [Rashid et al., 2007, 2011] were relatively consistent with the GISP2  $\delta^{18}\text{O}$  record (Figure 7, Panel b) [Grootes and Stuiver, 1999] suggesting a freshening as would be expected from an increased monsoonal response during this high latitude warming event. However, the  $\delta^{18}\text{O}_{\text{sw}}$  at the location of NGHP-01-19B, which lies north of the other two sites, remained fairly constant during the Bølling-Allerød. One would expect the increase in summer insolation experienced in the Northern Hemisphere during the Bølling-Allerød to pull the average annual position of the ITCZ farther north as the Asian landmass warmed. The regionally different hydrographic conditions

Figure 7. Comparison of Asian Monsoon region records since 22,000 BP. (a) June Insolation at 30°N (black line) [Berger and Loutre, 1991]. (b) GISP2  $\delta^{18}\text{O}$  [Grootes and Stuiver, 1999] (black line). (c) Chinese speleothem  $\delta^{18}\text{O}$ . Sanbao Cave: stalagmite SB26 (dark blue line), stalagmite SB10 (green line), stalagmite SB3 (magenta line) [Dykoski et al., 2005]. Dongge Cave: stalagmite D4 (light blue line) [Wang et al., 2008]. Hulu Cave: stalagmite PD (red line), stalagmite MSD (black line) [Wang et al., 2001]. (d) RC27-14 Arabian Sea  $\delta^{15}\text{N}_{\text{air}}$  (black line) [Altabet et al., 2002]. (e) NGHP-01-19B northwestern Bay of Bengal  $\delta^{18}\text{O}_{\text{sw}}$  (magenta squares, magenta line) [This study]. Black triangles indicating radiocarbon dates converted to calendar years BP (kyr). (f) 31/11 central Bay of Bengal  $\delta^{18}\text{O}_{\text{c}}$  (black crosses and black line) [Chauhan, 2003]. Black squares indicating radiocarbon dates converted to calendar years BP (kyr). (g\*) RC12-344 Andaman Sea  $\delta^{18}\text{O}_{\text{sw}}$  (black crosses and black line) [Rashid et al., 2007]. Black squares indicating radiocarbon dates converted to calendar years BP (kyr). (h\*) VM29-19 southwestern Bay of Bengal  $\delta^{18}\text{O}_{\text{sw}}$  (black crosses and black line) [Rashid et al., 2011]. Black squares indicating radiocarbon dates converted to calendar years BP (kyr). (i) Vostok  $\delta\text{D}$  (black line) [Petit et al., 2001]. The yellow shading indicates the Younger Dryas interval and the green shading indicates the Bølling-Allerød interval, both as recorded in GISP2  $\delta^{18}\text{O}$  [Grootes and Stuiver, 1999].

\*The data in panels (g) and (h) were digitized from the published figures because the original data were not available.





recorded in the Bay of Bengal during the Bølling-Allerød suggest that the ITCZ began to migrate northward during this event, passing over the source region for waters impacting the Andaman Sea and southwestern Bay sites, but not reaching the source region for the waters impacting the Mahanadi Basin site.

In the modern Bay of Bengal, surface water circulation during the period of maximum *G. ruber* abundance (June, July and August) indicates that *G. ruber* in the Mahanadi Basin likely record conditions related to Ganges-Brahmaputra runoff, perhaps with some minor contribution from the Mahanadi River (Figure 8). Conversely, the *G. ruber* at the southwestern Bay and Andaman Sea sites [Rashid *et al.*, 2007, 2011] record conditions more closely associated with peninsular Indian runoff. The Andaman

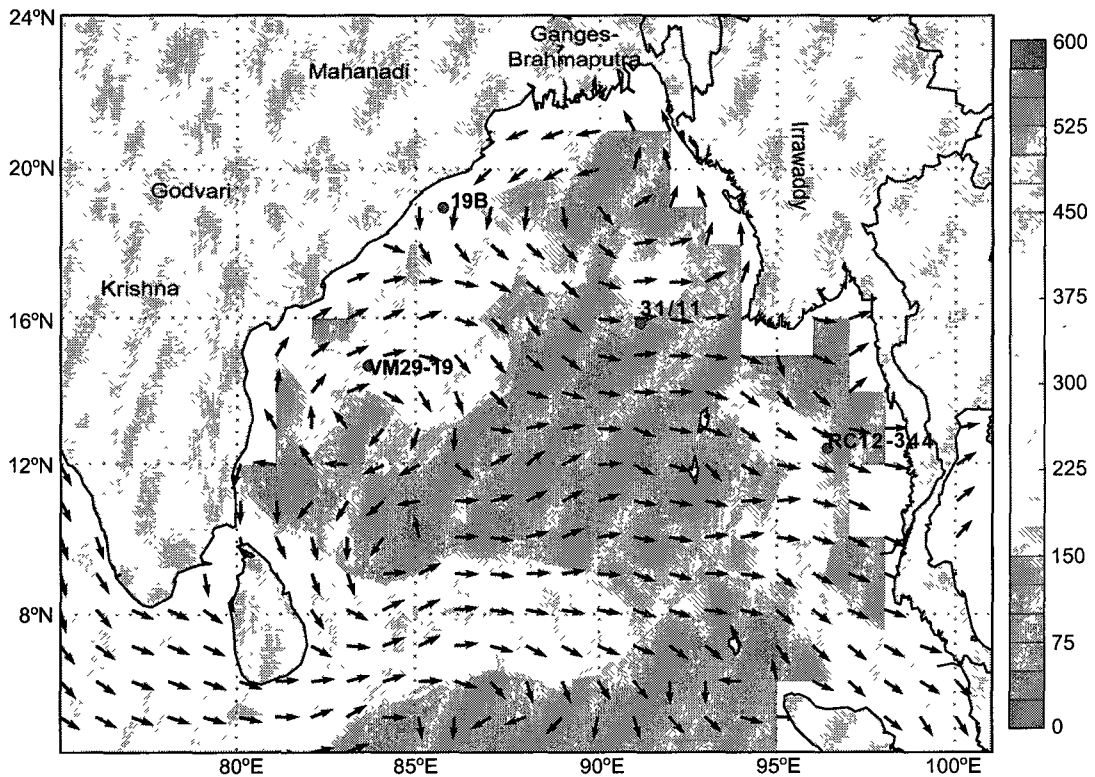


Figure 8. Map of Bay of Bengal showing surface (0 m) currents averaged over June, July and August (period of abundance maxima of *G. ruber*) in km per 10 days [Lumpkin and Garraffo, 2005] with circles indicating the locations of NGHP-01-19B, 31/11 [Chauhan, 2003], and VM29-19 [Rashid *et al.*, 2011], RC12-344 [Rashid *et al.*, 2007]. Blue lines indicate approximate locations of major rivers feeding into the Bay.

Sea site may also have some influence from the Irrawaddy River. Assuming a surface circulation in the Bay of Bengal during the deglaciation that was similar to the modern, it is possible that the southwestern Bay and Andaman Sea sites were bathed by isotopically light source waters from a region that was already experiencing an intensified monsoon, while waters at the Mahanadi Basin site remained isotopically heavy due to the weaker monsoon experienced in the region from which they originated.

During the Younger Dryas, the  $\delta^{18}\text{O}_{\text{sw}}$  values in the Andaman Sea and the southwestern Bay of Bengal [Rashid *et al.*, 2007, 2011] were relatively consistent with GISP2  $\delta^{18}\text{O}$  [Grootes and Stuiver, 1999], showing increases in  $\delta^{18}\text{O}_{\text{sw}}$ , as one would expect if monsoonal strength waned during this high latitude cooling event. However, the  $\delta^{18}\text{O}_{\text{sw}}$  in the Mahanadi Basin did not respond similarly during this time period. At approximately 12.5 ka, after the Younger Dryas response was well under way at the other two locations, the  $\delta^{18}\text{O}_{\text{sw}}$  in the Mahanadi Basin decreased (or freshened) and then oscillated until 8.7 ka. This high variability in the  $\delta^{18}\text{O}_{\text{sw}}$  of the Mahanadi Basin, anchored with radiocarbon dates converted to calendar age at the approximate beginning (12.5 ka) and middle (10.5 ka), is quite different from the other Bay of Bengal  $\delta^{18}\text{O}_{\text{sw}}$  records [e.g. Rashid *et al.*, 2007, 2011]. However, a *G. ruber*  $\delta^{18}\text{O}_{\text{c}}$  record from a core retrieved from the central Bay of Bengal (31/11) [Chauhan, 2003] reveals a similar response (Figure 7, Panel f). The similarities in these two records and their mutual difference with the records to the south [Rashid *et al.*, 2007, 2011] is likely due to surface circulation. The Mahanadi Basin and the site of core 31/11 lie within the cyclonic circulation in the modern northern bay during the summer monsoon months while the southwestern bay and Andaman Sea sites are located south of that circulation. If surface currents in the Bay of Bengal were similar during the Younger Dryas to those observed in the modern Bay, the Mahanadi Basin and central Bay sites may have remained isotopically distinct from the southwestern Bay and Andaman Sea.

The high frequency variability in the Mahanadi Basin  $\delta^{18}\text{O}_{\text{sw}}$  record may be a result

of the migration of the boundary between the gyre in the northern Bay and the northward currents to the south, leading to a shift in the source waters bathing the Mahanadi Basin during this time. *Chauhan* [2003] attributes the period of high  $\delta^{18}\text{O}_c$  variability seen in the central Bay of Bengal to changes in Himalayan climate (e.g. deglaciation, humidity/aridity related to the state of the monsoon) leading to changes in the fluvial runoff of the Ganges-Brahmaputra river system. This interpretation is supported by evidence suggesting the desiccation of Lake Victoria around 12.7 ka [*Johnson*, 1996], a time when both the Mahanadi Basin and central Bay record less freshwater input suggesting a weakened monsoon. Stratigraphic and seismic records of the evolution of the Bengal fan indicate increased monsoon intensity after 12.7 ka [*Weber et al.*, 1997] in agreement with the freshening recorded in both the central Bay and Mahanadi Basin at this time. The aridity suggested by both records around 10.5 ka is supported by evidence of Himalayan glaciers having descended to lower altitudes around the same time [*Phadtare*, 2002].

#### *Comparison to Asian Monsoon Region records*

The overall glacial to interglacial trend in  $\delta^{18}\text{O}_{\text{sw}}$  within the Bay of Bengal is consistent with the trend observed in Chinese speleothem  $\delta^{18}\text{O}$  (Figure 7, Panel c) [*Dykoski et al.*, 2005; *Wang et al.*, 2001, 2008], with both locations suggesting an increase in the intensity of the Asian monsoon since the last glacial period. Arabian Sea  $\delta^{15}\text{N}_{\text{air}}$ , which records the intensity of the denitrification associated with summer monsoon winds (Figure 7, Panel d) [*Altabet et al.*, 2002], also reveals an intensification of the Asian monsoon since the last glacial period. However, the  $\delta^{15}\text{N}_{\text{air}}$  record suggests that this shift did not begin in the Arabian Sea until the onset of the Bølling-Allerød warm period at approximately 14.9 kyrs BP. These differences in timing may suggest slightly different responses in the different branches of the monsoon to increases in NH summer insolation (Figure 6, Panel a) [*Berger and Loutre*, 1991]. The Mahanadi Basin  $\delta^{18}\text{O}_{\text{sw}}$  record must be extended through several precessional cycles before saying this with confidence.

The  $\delta^{18}\text{O}$  of Chinese speleothem calcite [Dykoski *et al.*, 2005; Wang *et al.*, 2001, 2008] shows clear Bølling-Allerød and Younger Dryas signals that agree with the  $\delta^{18}\text{O}$  of Greenland ice [Grootes and Stuiver, 1999], much like the  $\delta^{18}\text{O}_{\text{sw}}$  of the Andaman Sea and the southwestern Bay of Bengal [Rashid *et al.*, 2007, 2011]. However, the Mahanadi Basin  $\delta^{18}\text{O}_{\text{sw}}$  and the Arabian Sea  $\delta^{15}\text{N}_{\text{air}}$  [Altabet *et al.*, 2002] suggest very different Younger Dryas responses in these two locations. A similar pattern of deglaciation is seen in the  $\delta\text{D}$  record (inferred as temperature) of the Vostok ice core (Figure 7, Panel i) [Petit *et al.*, 2001] with a transition towards Holocene conditions beginning around this time.

## CHAPTER 6

### CONCLUSION

The new record of residual  $\delta^{18}\text{O}_{\text{sw}}$  from a marine sediment core retrieved from the Mahanadi Basin in the northwestern Bay of Bengal is one of very few records of its kind from this region of the world. The record indicates that the intensity of the Indian monsoon increased from the last glacial period to the present, consistent with other records from the Asian monsoon region. There are distinct differences between the new  $\delta^{18}\text{O}_{\text{sw}}$  record and the nearest records of  $\delta^{18}\text{O}_{\text{sw}}$  from the southwestern Bay of Bengal and Andaman Sea. While the  $\delta^{18}\text{O}_{\text{sw}}$  records from the Andaman Sea and southwestern Bay of Bengal [Rashid *et al.*, 2007, 2011] suggest that the intensity of the monsoon increased during the Bølling-Allerød, the Mahanadi Basin  $\delta^{18}\text{O}_{\text{sw}}$  record does not. This suggests that the ITCZ migrated northward during the Bølling-Allerød, but did not migrate northward enough to impact the source waters of the Mahanadi Basin. Furthermore, in the northwestern Bay of Bengal, the time period between 12.5 and 8.7 ka was a time of high-frequency variability in  $\delta^{18}\text{O}_{\text{sw}}$ . This variability is consistent with the variability observed in a similar record from the central Bay of Bengal [Chauhan, 2003], but is not consistent with variability observed in records from the Andaman Sea and the southwestern Bay. The differences in these responses are difficult to explain in terms of a shift in the northward extent of the ITCZ but may be attributable to differences in source waters affecting the different sites throughout the Bay.

This new record of  $\delta^{18}\text{O}_{\text{sw}}$  from the Mahanadi Basin exhibited some coherency with the record of GISP2  $\delta^{18}\text{O}$  [Grootes and Stuiver, 1999], Vostok  $\delta\text{D}$  [Petit *et al.*, 2001] and

summer insolation received at 30°N [*Berger and Loutre, 1991*]. It is clear from the new record that the monsoon was weaker during the last glacial and strengthened during the deglaciation. Throughout the Holocene the strength of the Indian monsoon appears to have been fairly constant with a slight decrease towards modern times, consistent with the slight decrease in NH summer insolation over the course of the Holocene. This record provides insight into the Indian monsoon and the greater Asian monsoon system from the Bay of Bengal, a region that is vital in our understanding of what forces the dynamics of the monsoon.

## LIST OF REFERENCES

- Altabet, M. A., M. J. Higginson, and D. W. Murray (2002), The effect of millennial-scale changes in Arabian Sea denitrification on atmospheric CO<sub>2</sub>, *Nature*, 415(6868), 159-162, doi: 10.1038/415159a.
- Antonov, J. I., R. A. Locarnini, T. P. Boyer, A. V. Mishonov, and H. E. Garcia (2006), *World Ocean Atlas 2005, Volume 2: Salinity*. S. Levitus, Ed. NOAA Atlas NESDIS 62, U.S. Government Printing Office, Washington, D.C., 182 pp.
- Arbuszewski, J., P. deMenocal, A. Kaplan, and E. Farmer (2010), On the fidelity of shell-derived  $\delta^{18}\text{O}_{\text{seawater}}$  estimates, *Earth Planet. Sci. Lett.*, 300(3-4), 185-196, doi: 10.1016/j.epsl.2010.10.035.
- Barnett, T., L. Dumenil, U. Schlese, and E. Roeckner (1988), The effect of Eurasian snow cover on global climate, *Science*, 239(4839), 504-507, doi: 10.1126/science.239.4839.504.
- Berger, A., and M. F. Loutre (1991), Insolation values for the climate of the last 10 million years, *Quaternary Sci. Rev.*, 10(4), 297-317, doi: 10.1016/0277-3791(91)90033-Q.
- Bond, G., W. Broecker, S. Johnson, J. McManus, L. Labeyrie, J. Jouzel, and G. Bonani (1993), Correlations between climate records from North Atlantic sediments and Greenland ice, *Nature*, 365(6442), 143-147, doi: 10.1038/365143a0.
- Boyle, E., and L. Keigwin (1985/86), Comparison of Atlantic and Pacific paleochemical records for the last 215,000 years: changes in deep ocean circulation and chemical inventories, *Earth Planet. Sci. Lett.*, 76(1-2), 135-150, doi: 10.1016/0012-821X(85)90154-2.
- Chauhan, O. S. (2003), Past 20,000-year history of Himalayan aridity: Evidence from oxygen isotope records in the Bay of Bengal, *Curr. Sci. India*, 84(1), 90-93.
- Cheng, H., R. Edwards, Y. Wan, X. Ko, Y. Ming, M. Kelly, X. Wang, C. Gallup, and W. Liu (2006), A penultimate glacial monsoon record from Hulu Cave and two-phase glacial terminations, *Geology*, 34(3), 217-220, doi: 10.1130/G22289.1.



- Clemens, S., W. Prell, D. Murray, G. Shimmield, and G. Weedon (1991), Forcing mechanisms of the Indian Ocean monsoon, *Nature*, 353(6346), 720-725, doi: 10.1038/353720a0.
- Clemens, S., and W. Prell (2003), A 350,000 year summer-monsoon multi-proxy stack from the Owen ridge, Northern Arabian sea, *Mar. Geol.*, 201(1-3), 35-51, doi: 10.1016/S0025-3227(03)00207-X.
- Clemens, S., and W. Prell (2007), The timing of orbital-scale Indian monsoon changes, *Quaternary Sci. Rev.*, 26(3-4), 275-278, doi: 10.1016/j.quascirev.2006.11.010.
- Collett, T., M. Riedel, J. Cochran, R. Boswell, J. Presley, P. Kumar, A. Sathe, A. Sethi, M. Lall, V. Sibal, and the NGHP Expedition 01 Scientists (2008), Site NGHP-01-19, in *Indian National Gas Hydrate Program: Expedition 01 Initial Reports*, U.S. Geol. Surv. and Directorate General of Hydrocarbons, Ministry of Petroleum & Natural Gas (India).
- Croll, J. (1875), *Climate and Time*, Appleton and Co., New York.
- Dekens, P., D. Lea, D. Pak, and H. Spero (2002), Core top calibration of Mg/Ca in tropical foraminifera: Refining paleotemperature estimation, *Geochem. Geophys. Geosys.*, 3, doi: 10.1029/2001GC000200.
- Delaygue, G., E. Bard, C. Rollion, J. Jouzel, M. Stievenard, J. Duplessy, and G. Ganssen (2001), Oxygen isotope/salinity relationship in the northern Indian Ocean, *J. Geophys. Res. [Oceans]*, 106(C3), 4565-4574.
- Dutta, K., R. Bhushan, and B. Somayajulu (2001), Delta R correction values for the northern Indian Ocean, *Radiocarbon*, 43(2A), 483-488.
- Dykoski, C., R. Edwards, H. Cheng, D. Yuan, Y. Cai, M. Zhang, Y. Lin, J. Qing, Z. An, and J. Revenaugh (2005), A high-resolution, absolute-dated Holocene and deglacial Asian monsoon record from Dongge Cave, China, *Earth Planet. Sci. Lett.*, 233(1-2), 71-86, doi: 10.1016/j.epsl.2005.01.036.
- Grootes, P. M. and M. Stuiver (1999), GISP2 Oxygen Isotope Data, doi: 10.1594/PANGAEA.56094.
- Guptha, M., W. Curry, V. Ittekkot, and A. Muralinath (1997), Seasonal variation in the flux of planktic foraminifera: Sediment trap results from the Bay of Bengal, northern Indian ocean, *J. Foramin. Res.*, 27(1), 5-19.
- Haug, G., K. Hughen, D. Sigman, L. Peterson, and U. Rohl (2001), Southward migration of the intertropical convergence zone through the Holocene, *Science*, 293(5533), 1304-1308.

- Hut, G. (1987), Consultants' Group Meeting on Stable Isotope Reference Samples for Geochemical and Hydrological Investigations, *IAEA*, Vienna 16-18 September, in *Report to the Director General*, 42 pp., International Atomic Energy Agency, Vienna.
- Krishna, K., and S. Rao (2009), ENSO-related modulation of coastal upwelling along the central east coast of India, *Atmos. Sci. Lett.*, *10*(1), 19-22, doi: 10.1002/asl.204.
- Kudrass, H., A. Hofmann, H. Dose, K. Emeis, and H. Erlenkeuser (2001), Modulation and amplification of climatic changes in the Northern Hemisphere by the Indian summer monsoon during the past 80 k.y., *Geology*, *29*(1), 63-66, doi: 10.1130/0091-7613(2001)029<0063:MAAOCC>2.0.CO;2.
- Kutzbach, J. (1981), Monsoon climate of the early Holocene: climate experiment with the Earth's orbital parameters for 9000 years ago, *Science*, *214*(4516), 59-61, doi: 10.1126/science.214.4516.59.
- Locarnini, R. A., A. V. Mishonov, J. I. Antonov, T. P. Boyer, and H. E. Garcia (2006), *World Ocean Atlas 2005, Volume 1: Temperature*. S. Levitus, Ed. NOAA Atlas NESDIS 61, U.S. Government Printing Office, Washington, D.C., 182 pp.
- Lumpkin, R. and Z. Garraffo (2005), Evaluating the Decomposition of Tropical Atlantic Drifter Observations, *J. Atmos. Oceanic Techn.* I, *22*, 1403-1415, doi: 10.1175/JTECH1793.1.
- Milankovitch, M. M. (1941), *Canon of insolation and the ice-age problem*, Koniglich Serbische Akademie, Beograd. [English translation by the Israel Program for Scientific Translations, published by the US Department of Commerce, and the National Science Foundation, Washington D.C. (1969).]
- Mulitza, S., D. Boltovskoy, B. Donner, H. Meggers, A. Paul, and G. Wefer (2003), Temperature: delta O-18 relationships of planktonic foraminifera collected from surface waters, *Palaeogeogr. Palaeoclimatol. Palaeoecol.*, *202*(1-2), 143-152, doi: 10.1016/S0031-0182(03)00633-3.
- Nurnberg, D., J. Bijma, and C. Hemleben (1996), Assessing the reliability of magnesium in foraminiferal calcite as a proxy for water mass temperatures, *Geochim. Cosmochim. Ac.*, *60*(5), 803-814, doi: 10.1016/0016-7037(96)82893-6.
- Overpeck, J., D. Anderson, S. Trumbore, and W. Prell (1996), The southwest Indian Monsoon over the last 18000 years, *Clim. Dynam.*, *12*(3), 213-225, doi: 10.1007/BF00211619.

- Petit, J. R., J. Jouzel, D. Raynaud, N. I. Barkov, J. M. Barnola, I. Basile, M. Bender, J. Chappellaz, J. Davis, G. Delaygue, M. Delmotte, V. M. Kotlyakov, M. Legrand, V. Lipenkov, C. Lorius, L. Pépin, C. Ritz, E. Saltzman, and M. Stievenard (2001), Vostok Ice Core Data for 420,000 Years, IGBP PAGES/World Data Center for Paleoclimatology Data Contribution Series #2001-076. NOAA/NGDC Paleoclimatology Program, Boulder CO, USA.
- Phadtare, N. R. (2002), Tectonics and Environment of the Himalaya: Comparison with other Regions, International conference on Quaternary Climate, Nainital, 16-17.
- Prell, W. L., and J. E. Kutzbach (1987), Monsoon Variability Over the Past 150,000 Years, *J. Geophys. Res.*, *92*(D7), PP. 8411-8425, doi: 198710.1029/JD092iD07p08411.
- Rashid, H., B. Flower, R. Poore, and T. Quinn (2007), A similar to 25 ka Indian Ocean monsoon variability record from the Andaman Sea, *Quaternary Sci. Rev.*, *26*(19-21), 2586-2597, doi: 10.1016/j.quascirev.2007.07.002.
- Rashid, H., E. England, L. Thompson, and L. Polyak (2011), Late Glacial to Holocene Indian Summer Monsoon Variability Based upon Sediment Records Taken from the Bay of Bengal, *Terr. Atmos. Ocean. Sci.*, *22*(2), 215-228, doi: 10.3319/TAO.2010.09.17.02(TibXS).
- Reimer, P. J., M. G. L. Baillie, E. Bard, A. Bayliss, J. W. Beck, P. G. Blackwell, C. Bronk Ramsey, C. E. Buck, G. S. Burr, R. L. Edwards, M. Friedrich, P. M. Grootes, T. P. Guilderson, I. Hajdas, T. J. Heaton, A. G. Hogg, K. A. Hughen, K. F. Kaiser, B. Kromer, F. G. McCormac, S. W. Manning, R. W. Reimer, D. A. Richards, J. R. Southon, S. Talamo, C. S. M. Turney, J. van der Plicht, and C. E. Weyhenmeyer (2009), INTERCAL09 and MARINE09 Radiocarbon age calibration curves, 0-50,000 years cal BP, *Radiocarbon*, *51*, 1111-1150.
- Rosenthal, Y., M. Field, and R. Sherrell (1999), Precise determination of element/calcium ratios in calcareous samples using sector field inductively coupled plasma mass spectrometry, *Anal. Chem.*, *71*(15), 3248-3253, doi: 10.1021/ac981410x.
- Schott, F., and J. McCreary (2001), The monsoon circulation of the Indian Ocean, *Prog. Oceanogr.*, *51*(1), 1-123, doi: 10.1016/S0079-6611(01)00083-0.
- Schott, F. A., S. P. Xie, and J. P. McCreary (2009), Indian Ocean circulation and climate variability, *Reviews of Geophysics*, *47*, RG1002, doi: 10.1029/2007RG000245.
- Southon, J., M. Kashgarian, M. Fontugne, B. Metivier, and W. Yim (2002), Marine reservoir corrections for the Indian Ocean and southeast Asia, *Radiocarbon*, *44*(1), 167-180.

- Stuiver, M., and P.J. Reimer (1993), Extended 14C database and revised CALIB radiocarbon calibration program, *Radiocarbon*, *35*, 215-230.
- Varkey, M., V. Murty, and A. Suryanarayana (1996), Physical oceanography of the Bay of Bengal and Andaman sea, *Oceanogr. Mar. Biol.*, *34*, 1-70.
- Waelbroeck, C., L. Labeyrie, E. Michel, J. Duplessy, J. McManus, K. Lambeck, E. Balbon, and M. Labracherie (2002), Sea-level and deep water temperature changes derived from benthic foraminifera isotopic records, *Quaternary Sci. Rev.*, *21*(1-3), 295-305, doi: 10.1016/S0277-3791(01)00101-9.
- Wang, Y., H. Cheng, R. Edwards, Z. An, J. Wu, C. Shen, and J. Dorale (2001), A high-resolution absolute-dated Late Pleistocene monsoon record from Hulu Cave, China, *Science*, *294*(5550), 2345-2348, doi: 10.1126/science.1064618.
- Wang, Y., H. Cheng, R. Edwards, Y. He, X. Kong, Z. An, J. Wu, M. Kelly, C. Dykoski, and X. Li (2005), The Holocene Asian monsoon: Links to solar changes and North Atlantic climate, *Science*, *308*(5723), 854-857, doi: 10.1126/science.1106296.
- Wang, Y., H. Cheng, R. Edwards, X. Kong, X. Shao, S. Chen, J. Wu, X. Jiang, X. Wang, and Z. An (2008), Millennial- and orbital-scale changes in the East Asian monsoon over the past 224,000 years, *Nature*, *451*(7182), 1090-1093, doi: 10.1038/nature06692.
- Weber, M. E., M. H. Wiedicke, H. R. Kudrass, C. Hubscher, and H. Erlenkeuser (1997), Active growth of the Bengal Fan during sea-level rise and highstand, *Geology*, *25*(4), 315-318, doi: 10.1130/0091-7613(1997)025<0315:AGOTBF>2.3.CO;2.
- You, Y. (1998), Intermediate water circulation and ventilation of the Indian Ocean derived from water-mass contributions, *J. Mar. Res.*, *56*(5), 1029-1067, doi: 10.1357/002224098765173455.

APPENDIX A

TABLES

Table 1. AMS dates and calendar ages\*.

Depth (cm)	MCD <sup>‡</sup> (cm)	Species	NOSAMS ID	AMS Date	AMS Error	1 or 2 $\sigma$	Age Lower (yrs BP)	Age Upper (yrs BP)	Age (yrs BP)
<i>NGHP-01-19B-1H-1</i>									
0-2	1	Mixed Planktics	OS-66064	1,850	35	1	1,333	1,436	1,384.5
						2	1,303	1,493	
<i>NGHP-01-19B-1H-2</i>									
44-45	194.5	<i>G. ruber</i> (white) and <i>G. sacculifer</i>	OS-82395	9,690	40	1	10,514	10,580	10,547
						2	10,474	10,637	
108-109	258.5	<i>G. ruber</i> (white)	OS-90201	11,050	45	1	12,406	12,447	
						1	12,530	12,561	12,545.5
						2	12,358	12,714	
<i>NGHP-01-19A-1H-3</i>									
23.8-25.8**	324.8	Mixed planktics	OS-66068	16,650	80	1	19,304	19,478	19,391
						1	19,494	19,544	
						2	18,932	19,161	
						2	19,210	19,581	
<i>NGHP-01-19B-1H-3</i>									
54-55	354.5	<i>G. ruber</i> (white)	OS-89468	22,900	80	1	26,913	27,100	
						1	27,154	27,564	27,359
						2	26,732	27,738	

\*AMS radiocarbon dates were converted to calendar age BP (1950) using CALIB 6.0 [Stuiver and Reimer, 1993], the Marine09 dataset [Reimer et al., 2009] and the standard reservoir correction of 400 year.

<sup>‡</sup>Mean Composite Depth

\*\*Original depth in NGHP-01-19A-1H-3 of 20-22 cm corrected by addition of 3.8 cm to equivalent NGHP-01-19B-1H-3 depth by comparison of magnetic susceptibility records of both cores.

Table 2. NGHP 01-19B *G. ruber* (white) data.

Depth (cm)	MCD‡ (cm)	Age (yrs BP)	<i>G. ruber</i> picked (212-250µm)	<i>G. ruber</i> picked (250-300µm)	Total <i>G. ruber</i> picked	Mean test weight (µg)
<i>NGHP-01-19B-1H-1</i>						
8-10	9	1,763	25	25	50	7.87
16-18	17	2,142	4	1	5	7.60
24-26	25	2,521	23	17	40	7.02
32-34	33	2,900	13	7	20	7.30
40-42	41	3,279	7	5	12	6.33
48-50	49	3,657	10	10	20	7.92
56-58	57	4,036	12	6	18	7.13
64-66	65	4,415	13	17	30	8.00
72-74	73	4,794	13	11	24	7.80
79-81	80	5,125	7	10	17	7.98
88-90	89	5,551	7	5	12	6.57
96-98	97	5,930	6	4	10	7.50
104-106	105	6,309	5	6	11	7.49
112-114	113	6,688	41	20	61	7.64
120-122	121	7,067	6	5	11	6.66
128-130	129	7,445	14	10	24	8.00
136-138	137	7,824	20	24	44	7.48
144-146	145	8,203	39	30	69	7.34
<i>NGHP-01-19B-1H-2</i>						
4-6	155	8,677	29	20	49	7.87
12-14	163	9,055	24	21	45	8.06
20-22	171	9,434	6	5	11	6.85
28-30	179	9,813	50	50	100	8.20
36-38	187	10,192	44	29	73	9.12
44-45	194.5	10,547	88		88	7.61
45-46	195.5	10,578	56	36	92	8.82
52-54	203	10,812	50	22	72	7.60
60-62	211	11,062	57	34	91	8.15
64-66	215	11,187	26	24	50	10.38
68-70	219	11,312	54	46	100	8.34
72-74	223	11,437	16	21	37	9.50
76-78	227	11,562	36	31	67	8.30
80-82	231	11,687	3	3	6	9.05
84-86	235	11,812	42	54	96	8.87
90-92	241	11,999	9	19	28	9.85
92-94	243	12,061	48	52	100	7.74
98-100	249	12,249	57	33	90	8.77
100-101	250.5	12,296	84		84	7.14
101-102	251.5	12,327	90		90	6.18
105-106	255.5	12,452	91		91	7.55
108-109	258.5	12,546	100		100	6.52
112-113	262.5	12,959	100		100	7.45
116-117	266.5	13,372	78		78	6.98
120-121	270.5	13,785	100		100	6.66
124-125	274.5	14,198	83		83	7.22
128-129	278.5	14,611	100		100	7.73
132-133	282.5	15,024	94		94	7.96
136-137	286.5	15,437	100		100	7.76

Table 2. (cont.).

Depth (cm)	MCD <sup>‡</sup> (cm)	Age (yrs BP)	<i>G. ruber</i> picked (212-250µm)	<i>G. ruber</i> picked (250-300µm)	Total <i>G.</i> <i>ruber</i> picked	Mean test weight (µg)
<i>NGHP-01-19B-1H-2</i>						
140-141	290.5	15,850	88		88	7.31
144-145	294.5	16,263	100		100	8.64
148-149	298.5	16,676	100		100	7.52
<i>NGHP-01-19B-1H-3</i>						
2-3	302.5	17,089	100		100	8.16
6-7	306.5	17,502	100		100	8.47
10-11	310.5	17,915	100		100	7.89
14-15	314.5	18,328	100		100	7.66
18-19	318.5	18,741	100		100	8.45
22-23	322.5	19,154	100		100	7.03
30-32	330.5	20,920	100		100	7.74
38-39	338.5	23,066	100		100	7.88
46-47	346.5	25,213	100		100	6.57
54-55	354.5	27,359	100		100	7.55
62-63	362.5	29,352	94		94	7.98
70-71	370.5	31,423	100		100	7.88

<sup>‡</sup>Mean Composite Depth



Table 3. NGHP 01-19B *G. ruber* (white) Mg/Ca data.

Depth (cm)	MCD‡ (cm)	Age (yrs BP)	Mean Test Weight (µg)	[Ca] (ppm)	Mg/Ca (mmol mol <sup>-1</sup> )	Mean Mg/Ca (mmol mol <sup>-1</sup> )	Temperature (°C)*
<i>NGHP-01-19B-1H-1</i>							
8-10	9	1,763	7.9	19.8	4.79	4.68	27.9
8-10	9	1,763	7.9	41.6	4.57		
24-26	25	2,521	7.0	35.9	4.61	4.52	27.5
24-26	25	2,521	7.0	23.8	4.43		
48-50	49	3,657	7.9	32.1	4.37	4.37	27.1
56-58	57	4,036	7.1	21.2	4.17	4.17	26.6
64-66	65	4,415	8.0	25.2	4.35	4.35	27.1
72-74	73	4,794	7.8	37.7	4.72	4.72	28.0
79-81	80	5,125	8.0	36.8	4.48	4.48	27.4
96-98	97	5,930	7.5	10.5	4.20	4.20	26.7
104-106	105	6,309	7.5	17.1	4.55	4.55	27.6
112-114	113	6,688	7.6	19.1	4.04	4.18	26.6
112-114	113	6,688	7.6	70.3	4.32		
128-130	129	7,445	8.0	25.5	4.18	4.18	26.6
136-138	137	7,824	7.5	4.4	4.12	4.16	26.6
136-138	137	7,824	7.5	44.7	4.21		
144-146	145	8,203	7.3	26.6	4.23	4.28	26.9
144-146	145	8,203	7.3	37.9	4.33		
<i>NGHP-01-19B-1H-2</i>							
4-6	155	8,677	7.9	32.6	3.99	4.04	26.3
4-6	155	8,677	7.9	22.5	4.10		
12-14	163	9,055	8.1	50.4	4.46	4.66	27.9
12-14	163	9,055	8.1	41.7	4.86		
20-22	171	9,434	6.9	8.9	5.06	5.06	28.8
28-30	179	9,813	8.2	13.7	4.96	4.79	28.2
28-30	179	9,813	8.2	36.8	4.62		
36-38	187	10,192	9.1	13.8	4.10	4.12	26.5
36-38	187	10,192	9.1	22.7	4.15		
44-45	194.5	10,547	7.6	8.1	4.11	4.14	26.5
44-45	194.5	10,547	7.6	19.5	4.18		
45-46	195.5	10,578	8.8	16.0	4.61	4.92	28.4
45-46	195.5	10,578	8.8	34.7	5.23		
52-54	203	10,812	7.6	55.6	4.77	4.59	27.7
52-54	203	10,812	7.6	75.5	4.40		
60-62	211	11,062	8.1	43.3	4.58	4.52	27.5
60-62	211	11,062	8.1	48.0	4.47		
68-70	219	11,312	8.3	46.7	4.07	4.12	26.5
68-70	219	11,312	8.3	29.5	4.18		
76-78	227	11,562	8.3	55.4	4.19	4.10	26.4
76-78	227	11,562	8.3	61.4	4.01		
84-86	235	11,812	8.9	52.2	4.39	4.49	27.4
84-86	235	11,812	8.9	54.1	4.58		
92-94	243	12,061	7.7	29.8	4.13	4.30	27.0
92-94	243	12,061	7.7	37.6	4.48		
100-101	250.5	12,296	7.1	42.5	4.31	4.42	27.3
100-101	250.5	12,296	7.1	48.0	4.53		
101-102	251.5	12,327	6.2	24.0	3.84	3.97	26.1
101-102	251.5	12,327	6.2	25.3	4.09		

Table 3. (cont.).

Depth (cm)	MCD‡ (cm)	Age (yrs BP)	Mean Test Weight (µg)	[Ca] (ppm)	Mg/Ca (mmol mol <sup>-1</sup> )	Mean Mg/Ca (mmol mol <sup>-1</sup> )	Temperature (°C)*
<i>NGHP-01-19B-1H-2</i>							
108-109	258.5	12,546	6.5	28.2	3.81	3.93	26.0
108-109	258.5	12,546	6.5	38.2	4.05		
116-117	266.5	13,372	7.0	49.9	4.04	4.05	26.3
116-117	266.5	13,372	7.0	64.3	4.06		
124-125	274.5	14,198	7.2	55.0	4.25	4.22	26.8
124-125	274.5	14,198	7.2	59.5	4.20		
132-133	282.5	15,024	8.0	37.8	4.18	4.06	26.3
132-133	282.5	15,024	8.0	20.6	3.93		
140-141	290.5	15,850	7.3	43.6	4.16	4.11	26.4
140-141	290.5	15,850	7.3	42.8	4.05		
148-149	298.5	16,676	7.5	68.4	4.08	4.12	26.5
148-149	298.5	16,676	7.5	40.0	4.15		
<i>NGHP-01-19B-1H-3</i>							
6-7	306.5	17,502	8.5	72.9	3.97	3.99	26.1
6-7	306.5	17,502	8.5	50.5	4.01		
14-15	314.5	18,328	7.7	67.6	3.88	3.81	25.6
14-15	314.5	18,328	7.7	47.9	3.74		
22-23	322.5	19,154	7.0	68.5	3.83	3.80	25.6
22-23	322.5	19,154	7.0	56.0	3.77		
30-32	330.5	20,920	7.7	48.4	3.91	3.89	25.8
30-32	330.5	20,920	7.7	78.8	3.87		
38-39	338.5	23,066	7.9	73.3	4.22	4.13	26.5
38-39	338.5	23,066	7.9	36.6	4.03		
46-47	346.5	25,213	6.6	40.8	3.80	3.78	25.5
46-47	346.5	25,213	6.6	21.9	3.76		
54-55	354.5	27,359	7.6	41.9	3.55	3.58	24.9
54-55	354.5	27,359	7.6	39.5	3.61		
62-63	362.5	29,352	8.0	28.0	3.93	3.93	25.9
62-63	362.5	29,352	8.0	43.0	3.93		
70-71	370.5	31,423	7.9	22.6	3.82	3.85	25.7
70-71	370.5	31,423	7.9	25.4	3.88		

‡Mean Composite Depth

\*Temperatures were calculated using the *G. ruber* (white) 250-350 µm equation of Dekens *et al.* [2002].

Table 4. NGHP 01-19B G. ruber (white)  $\delta^{18}\text{O}$  data.

Depth (cm)	MCD <sup>†</sup> (cm)	Age (yrs BP)	$\delta^{18}\text{O}$ (‰)	Mean $\delta^{18}\text{O}$ (‰ VPBD)	Mean $\delta^{18}\text{O}$ (‰ VSMOW)*
<i>NGHP-01-19B-1H-1</i>					
8-10	9	1,763	-2.96	-2.96	-2.69
8-10	9	1,763	-2.95		
16-18	17	2,142	-2.94	-2.94	-2.67
24-26	25	2,521	-3.10	-3.13	-2.86
24-26	25	2,521	-3.15		
32-34	33	2,900	-3.00	-3.00	-2.73
40-42	41	3,279	-3.03	-3.03	-2.76
48-50	49	3,657	-2.92	-2.92	-2.65
56-58	57	4,036	-3.04	-3.04	-2.77
64-66	65	4,415	-2.94	-2.94	-2.67
72-74	73	4,794	-3.06	-3.06	-2.79
79-81	80	5,125	-3.22	-3.22	-2.95
88-90	89	5,551	-3.09	-3.09	-2.82
96-98	97	5,930	-3.02	-3.02	-2.75
104-106	105	6,309	-3.10	-3.10	-2.83
112-114	113	6,688	-2.86	-2.93	-2.66
112-114	113	6,688	-3.00		
120-122	121	7,067	-2.87	-2.87	-2.60
128-130	129	7,445	-3.15	-3.15	-2.88
136-138	137	7,824	-2.80	-2.80	-2.53
136-138	137	7,824	-2.80		
144-146	145	8,203	-3.02	-2.98	-2.71
144-146	145	8,203	-2.94		
<i>NGHP-01-19B-1H-2</i>					
4-6	155	8,677	-3.16	-3.10	-2.83
4-6	155	8,677	-3.04		
12-14	163	9,055	-3.15	-3.07	-2.80
12-14	163	9,055	-3.00		
20-22	171	9,434	-3.33	-3.33	-3.06
28-30	179	9,813	-2.94	-2.93	-2.66
28-30	179	9,813	-2.91		
36-38	187	10,192	-3.35	-3.35	-3.08
36-38	187	10,192	-3.35		
44-45	194.5	10,547	-2.49	-2.29	-2.02
44-45	194.5	10,547	-2.08		
45-46	195.5	10,578	-2.55	-2.62	-2.35
45-46	195.5	10,578	-2.68		
52-54	203	10,812	-3.09	-3.09	-2.82
52-54	203	10,812	-3.09		
60-62	211	11,062	-3.47	-3.33	-3.06
60-62	211	11,062	-3.19		
64-66	215	11,187	-3.22	-3.34	-3.07
64-66	215	11,187	-3.47		
68-70	219	11,312	-1.58	-1.65	-1.38
68-70	219	11,312	-1.72		
72-74	223	11,437	-2.95	-3.02	-2.75
72-74	223	11,437	-3.08		

Table 4. (cont.).

Depth (cm)	MCD <sup>†</sup> (cm)	Age (yrs BP)	$\delta^{18}\text{O}$ (‰)	Mean $\delta^{18}\text{O}$ (‰ VPBD)	Mean $\delta^{18}\text{O}$ (‰ VSMOW)*
<i>NGHP-01-19B-1H-2</i>					
76-78	227	11,562	-2.87	-2.91	-2.64
76-78	227	11,562	-2.94		
80-82	231	11,687	-3.03	-3.03	-2.76
84-86	235	11,812	-3.34	-3.22	-2.95
84-86	235	11,812	-3.10		
90-92	241	11,999	-2.96	-2.88	-2.61
90-92	241	11,999	-2.80		
92-94	243	12,061	-2.25	-2.46	-2.19
92-94	243	12,061	-2.67		
98-100	249	12,249	-2.24	-2.18	-1.91
98-100	249	12,249	-2.11		
100-101	250.5	12,296	-2.51	-2.44	-2.17
100-101	250.5	12,296	-2.38		
101-102	251.5	12,327	-2.19	-2.17	-1.90
101-102	251.5	12,327	-2.16		
105-106	255.5	12,452	-1.85	-1.73	-1.46
105-106	255.5	12,452	-1.61		
108-109	258.5	12,546	-1.63	-1.60	-1.33
108-109	258.5	12,546	-1.57		
112-113	262.5	12,959	-1.53	-1.53	-1.26
112-113	262.5	12,959	-1.53		
116-117	266.5	13,372	-1.64	-1.61	-1.34
116-117	266.5	13,372	-1.57		
120-121	270.5	13,785	-1.61	-1.69	-1.42
120-121	270.5	13,785	-1.77		
124-125	274.5	14,198	-1.55	-1.63	-1.36
124-125	274.5	14,198	-1.71		
128-129	278.5	14,611	-1.56	-1.42	-1.15
128-129	278.5	14,611	-1.29		
132-133	282.5	15,024	-1.33	-1.27	-1.00
132-133	282.5	15,024	-1.21		
136-137	286.5	15,437	-1.04	-1.04	-0.77
136-137	286.5	15,437	-1.04		
140-141	290.5	15,850	-1.15	-1.14	-0.87
140-141	290.5	15,850	-1.13		
144-145	294.5	16,263	-0.85	-0.84	-0.57
144-145	294.5	16,263	-0.83		
148-149	298.5	16,676	-0.81	-0.82	-0.55
148-149	298.5	16,676	-0.82		
<i>NGHP-01-19B-1H-3</i>					
2-3	302.5	17,089	-0.91	-0.91	-0.64
2-3	302.5	17,089	-0.91		
6-7	306.5	17,502	-0.95	-0.90	-0.63
6-7	306.5	17,502	-0.84		
10-11	310.5	17,915	-0.92	-1.00	-0.73
10-11	310.5	17,915	-1.09		
14-15	314.5	18,328	-0.95	-0.91	-0.64
14-15	314.5	18,328	-0.88		

Table 4. (cont.).

Depth (cm)	MCD <sup>‡</sup> (cm)	Age (yrs BP)	$\delta^{18}\text{O}$ (‰)	Mean $\delta^{18}\text{O}$ (‰ VPBD)	Mean $\delta^{18}\text{O}$ (‰ VSMOW)*
<i>NGHP-01-19B-1H-3</i>					
18-19	318.5	18,741	-1.05	-0.97	-0.70
18-19	318.5	18,741	-0.89		
22-23	322.5	19,154	-1.16	-1.12	-0.85
22-23	322.5	19,154	-1.07		
30-32	330.5	20,920	-1.13	-1.15	-0.88
30-32	330.5	20,920	-1.17		
38-39	338.5	23,066	-1.13	-1.09	-0.82
38-39	338.5	23,066	-1.05		
46-47	346.5	25,213	-1.09	-1.13	-0.86
46-47	346.5	25,213	-1.17		
54-55	354.5	27,359	-1.04	-1.12	-0.85
54-55	354.5	27,359	-1.19		
62-63	362.5	29,352	-1.17	-1.15	-0.88
62-63	362.5	29,352	-1.14		
70-71	370.5	31,423	-1.47	-1.36	-1.09
70-71	370.5	31,423	-1.24		

<sup>‡</sup>Mean Composite Depth

\* $\delta^{18}\text{O}$  values relative to VPBD were converted to be relative to VSMOW by adding 0.27‰ to all

Table 5. NGHP 01-19B G. ruber (white) residual seawater  $\delta^{18}\text{O}$  data.

MCD <sup>‡</sup> (cm)	Age (yrs BP)	Mean $\delta^{18}\text{O}_c$		Mean $\delta^{18}\text{O}_{sw}$	
		Uncorrected (‰)	Ice Volume Correction* (‰)	Ice Volume Corrected (‰)	Corrected** (‰)
<i>NGHP-01-19B-1H-1</i>					
9	1,763	-2.69	0.00	-2.69	0.40
25	2,521	-2.86	0.00	-2.86	0.14
49	3,657	-2.65	0.01	-2.66	0.25
57	4,036	-2.77	0.01	-2.78	0.01
65	4,415	-2.67	0.02	-2.69	0.22
73	4,794	-2.79	0.02	-2.81	0.30
80	5,125	-2.95	0.02	-2.97	0.00
97	5,930	-2.75	0.03	-2.79	0.03
105	6,309	-2.83	0.04	-2.87	0.15
113	6,688	-2.66	0.05	-2.70	0.10
129	7,445	-2.88	0.07	-2.95	-0.14
137	7,824	-2.53	0.08	-2.61	0.19
145	8,203	-2.71	0.10	-2.81	0.05
<i>NGHP-01-19B-1H-2</i>					
155	8,677	-2.83	0.14	-2.97	-0.25
163	9,055	-2.80	0.17	-2.98	0.10
171	9,434	-3.06	0.20	-3.26	0.02
179	9,813	-2.66	0.25	-2.90	0.24
187	10,192	-3.08	0.29	-3.37	-0.60
194.5	10,547	-2.02	0.33	-2.35	0.43
195.5	10,578	-2.35	0.33	-2.68	0.53
203	10,812	-2.82	0.36	-3.18	-0.14
211	11,062	-3.06	0.39	-3.45	-0.45
219	11,312	-1.38	0.42	-1.80	0.97
227	11,562	-2.64	0.45	-3.09	-0.33
235	11,812	-2.95	0.48	-3.43	-0.45
243	12,061	-2.19	0.51	-2.70	0.17
250.5	12,296	-2.17	0.54	-2.72	0.23
251.5	12,327	-1.90	0.55	-2.45	0.22
258.5	12,546	-1.33	0.58	-1.91	0.74
266.5	13,372	-1.34	0.67	-2.01	0.71
274.5	14,198	-1.36	0.77	-2.13	0.70
282.5	15,024	-1.00	0.85	-1.85	0.88
290.5	15,850	-0.87	0.91	-1.78	0.98
298.5	16,676	-0.55	0.95	-1.50	1.26

Table 5. (cont.).

MCD <sup>‡</sup> (cm)	Age (yrs BP)	Mean $\delta^{18}\text{O}_c$		Mean $\delta^{18}\text{O}_{sw}$	
		Uncorrected (‰)	Ice Volume Correction* (‰)	Ice Volume Corrected (‰)	Corrected** (‰)
<i>NGHP-01-19B-1H-3</i>					
306.5	17,502	-0.63	0.99	-1.62	1.07
314.5	18,328	-0.64	1.01	-1.66	0.91
322.5	19,154	-0.85	1.03	-1.87	0.69
330.5	20,920	-0.88	1.03	-1.91	0.71
338.5	23,066	-0.82	1.00	-1.82	0.95
346.5	25,213	-0.86	0.93	-1.79	0.76
354.5	27,359	-0.85	0.85	-1.69	0.71
362.5	29,352	-0.88	0.74	-1.62	1.01
370.5	31,423	-1.09	0.68	-1.76	0.82

<sup>‡</sup>Mean Composite Depth

\*Ice Volume Correction from *Waelbroeck et al.* [2002]

\*\* $\delta^{18}\text{O}_{sw}$  calculated using the *G. ruber* (white) equation of *Mulitza et al.* [2003]

APPENDIX B

PICTURES





Photo 1. Four *G. ruber* (white) picked from NGHP-01-19B-1H-1, 8 – 10 cm.

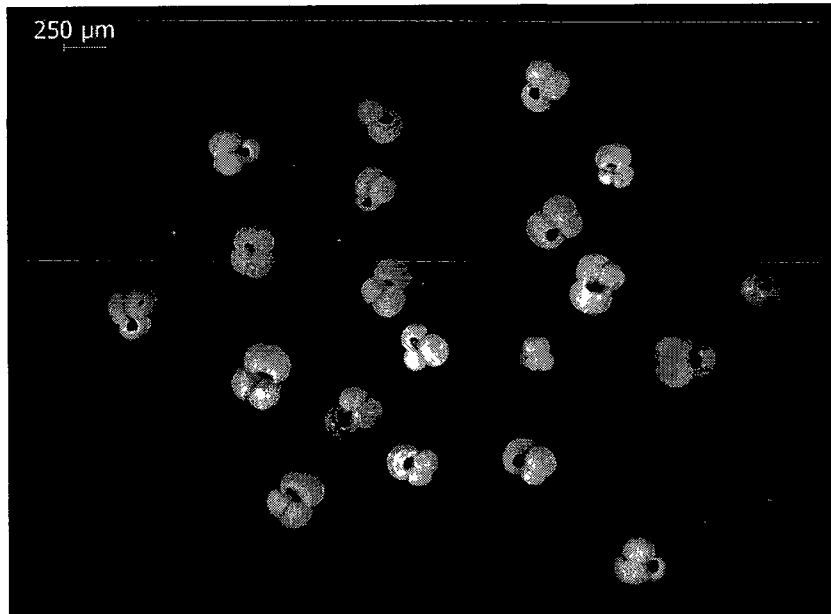


Photo 2. Twenty *G. ruber* (white) picked from NGHP-01-19B-1H-1, 48 – 50 cm.



Photo 3. Individual *G. ruber* (white) picked from NGHP-01-19B-1H-1, 48 – 50 cm.

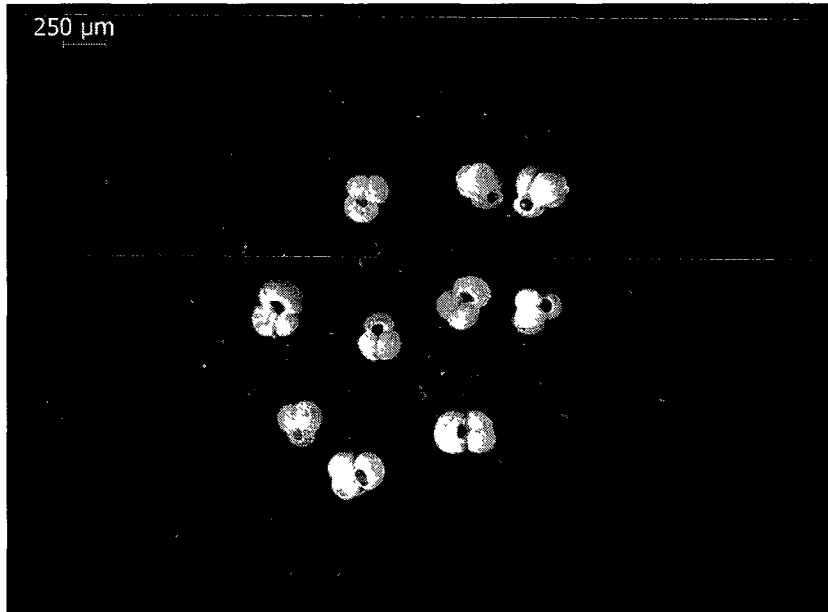


Photo 4. Ten *G. ruber* (white) picked from NGHP-01-19B-1H-1, 104 – 106 cm.

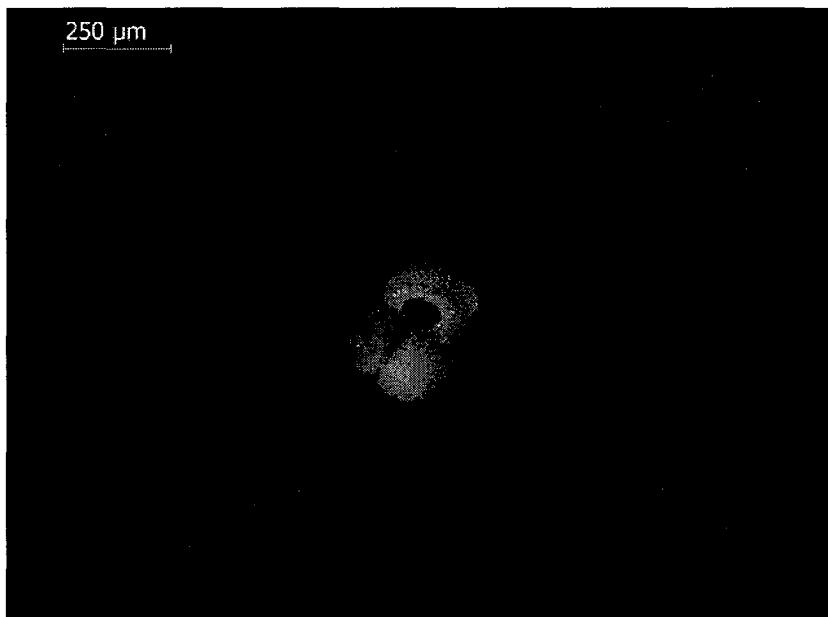


Photo 5. Individual *G. ruber* (white) picked from NGHP-01-19B-1H-1, 104 – 106 cm.

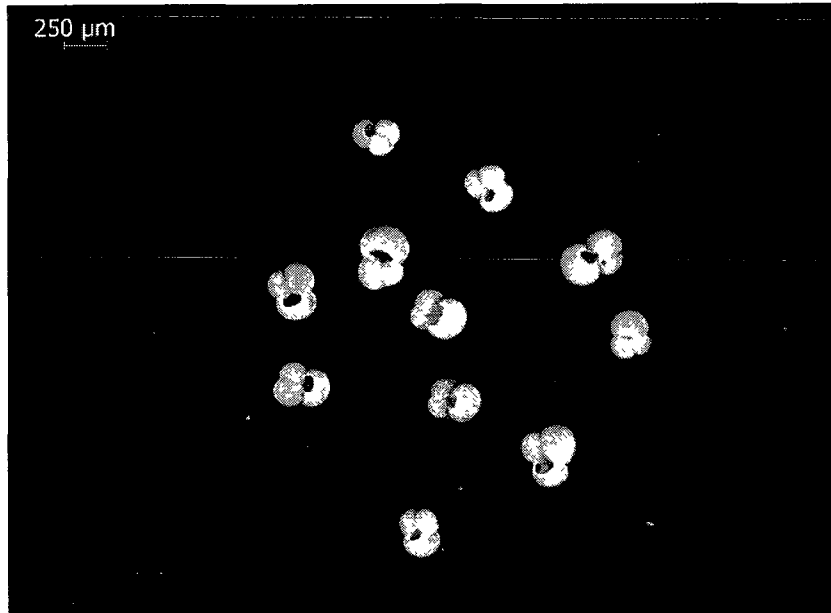


Photo 6. Eleven *G. ruber* (white) picked from NGHP-01-19B-1H-1, 120 – 122 cm.



Photo 7. Individual *G. ruber* (white) picked from NGHP-01-19B-1H-1, 120 – 122 cm.

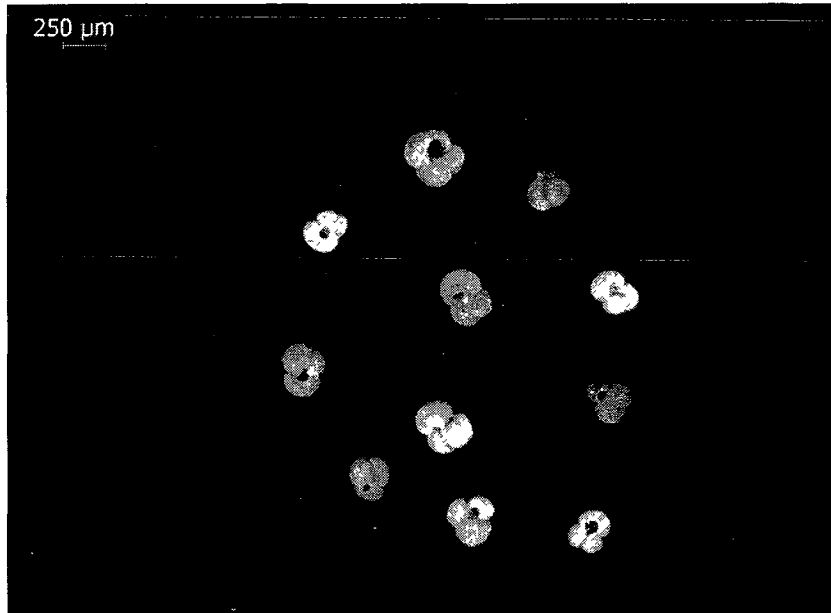


Photo 8. Eleven *G. ruber* (white) picked from NGHP-01-19B-1H-2, 170 – 172 cm.



Photo 9. Individual *G. ruber* (white) picked from NGHP-01-19B-1H-2, 170 – 172 cm.

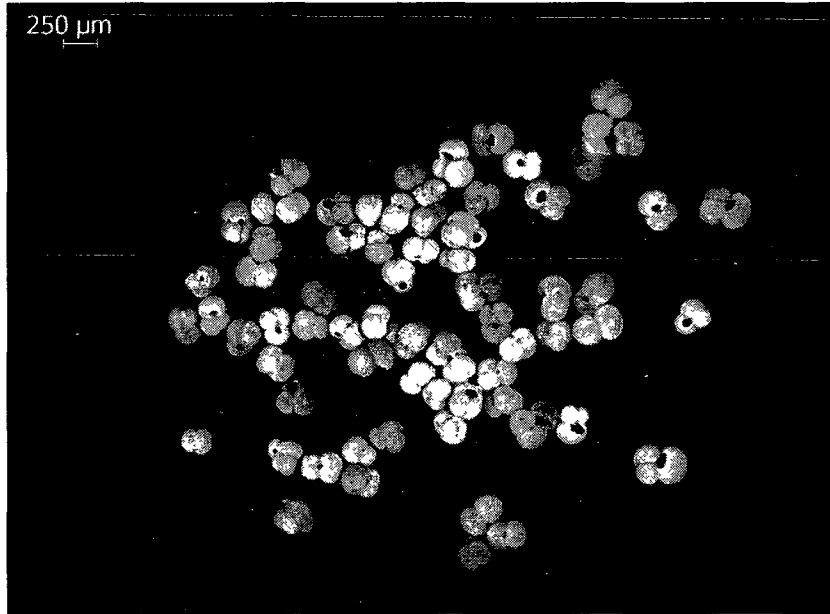


Photo 10. Seventy-two *G. ruber* (white) picked from NGHP-01-19B-1H-2, 202 – 204 cm.

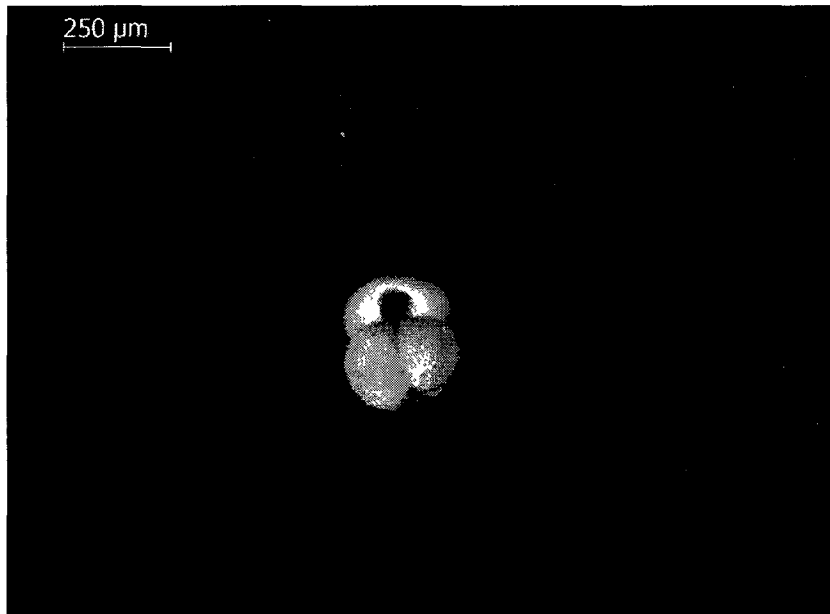


Photo 11. Individual *G. ruber* (white) picked from NGHP-01-19B-1H-2, 202 – 204 cm.

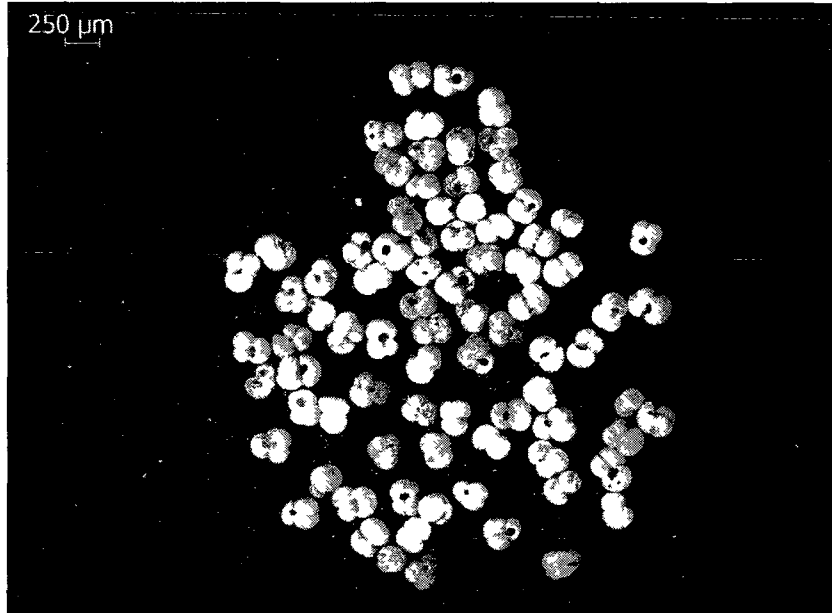


Photo 12. Eighty-four *G. ruber* (white) picked from NGHP-01-19B-1H-2, 250 – 251 cm.

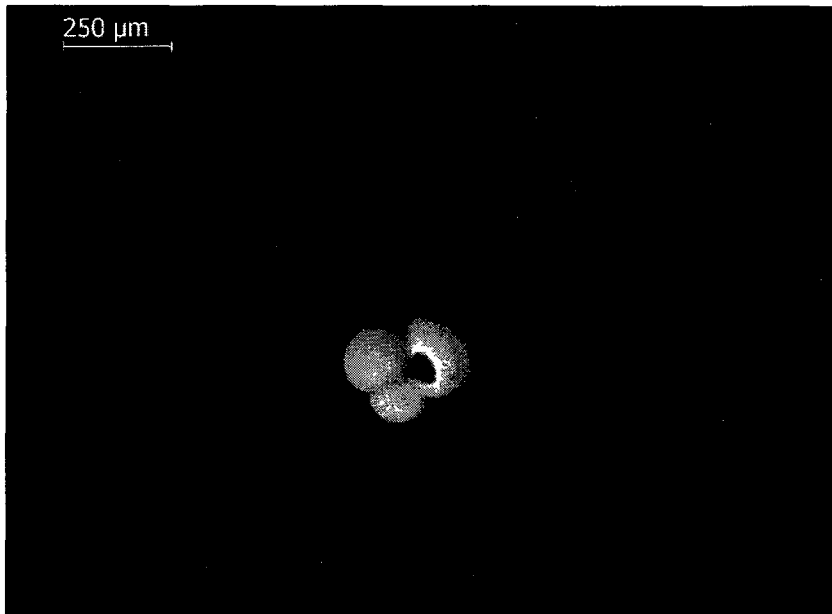


Photo 13. Individual *G. ruber* (white) picked from NGHP-01-19B-1H-2, 250 – 251 cm.